ELSEVIER

International Journal of Solids and Structures 41 (2004) 1697–1724

INTERNATIONAL JOURNAL OF SOLIDS and STRUCTURES

www.elsevier.com/locate/ijsolstr

High-order free vibration of sandwich panels with a flexible core

Y. Frostig [a,*], O.T. Thomsen [b]

[a] *Faculty of Civil and Environmental Engineering, Department of Structural Engineering, Technion-Israel Institute of Technology, Haifa 32000, Israel*

[b] *Institute of Mechanical Engineering, Aalborg University, DK-9220 Aalborg, Denmark*

Received 1 December 2002; received in revised form 3 September 2003

Abstract

Free vibration analysis of sandwich panels with a flexible core based on the high-order sandwich panel theory approach is presented. The mathematical formulation uses the Hamilton principle and includes derivation of the governing equations along with the appropriate boundary conditions. The formulation embodies a rigorous approach for the free vibration analysis of sandwich plates with a general construction, having high-order effects owing to the non-linear patterns of the in-plane and the vertical displacements of the core through its height. As such, it improves on the available classical and high-order theories. The formulation uses the classical thin plate theory for the face sheets and a three-dimensional elasticity theory or equivalent one for the core. The analyses are valid for any type of loading scheme, localized as well as distributed, and distinguish between loads applied at the upper or the lower face. It can also deal with any type of boundary conditions that may be different at the upper and the lower face sheets at the same edge. The effects of the rotary inertia of the various constituents of the sandwich construction are included. Two types of computational models are considered. The first model uses the vertical shear stresses in the core in addition to the displacements of the upper and the lower face sheets as its unknowns. The second model assumes a polynomial description of the displacement fields in the core that is based on the displacement fields of the first model. In this case the unknowns are the coefficients of these polynomials in addition to the displacements of the various face sheets. The two computational models have been validated numerically through a very good comparison with the well known classical and high-order plate theories. The numerical study consists of free vibration eigenmodes of two typical simply-supported panels, including higher modes that cannot be detected by other high-order computational models, and a parametric study that compares the results of the various computational models and the first-order shear deformable results.

* Corresponding author. Tel.: +97-248293046; fax: +97-248295697.
E-mail address: cvrfros@techunix.technion.ac.il (Y. Frostig).

0020-7683/$ - see front matter © 2003 Elsevier Ltd. All rights reserved.
doi:10.1016/j.ijsolstr.2003.09.051

1. Introduction

Modern sandwich panels are light with a high strength to weight ratio, and nowadays are being used in aerospace, naval, transportation and civil engineering industries. They are usually made of two metallic or composite laminated materials face sheets and a foam or low strength honeycomb core. This type of core is flexible in all directions and very flexible relative to the face sheets. As such, its behavior is associated with localized effects in the form of localized displacements and stresses which affect the safety of the overall panel. These effects lead to unidentical displacement patterns through the depth of the panel where the displacements of the upper face sheet differ from those of the lower one. They are associated with changes in the height of the core and the plane of section of the core taking on a non-linear pattern, rather than a linear one, as used by many researchers. Free vibration modes of such panels consist of overall mode and localized ones or through the thickness that the classical plate and sandwich panel theories lack to detect.

Many researchers have studied sandwich panels with traditional honeycomb cores that are infinitely stiff in the vertical direction, very flexible in the in-plane direction, and whose section plane remains linear or takes a "zig-zag" shape under static and dynamic loads. Many of these research works are described in textbooks, such as: Allen (1966), Plantema (1966) from the late sixties, Zenkert (1995) and Vinson (1999) from the nineties and a thorough review on sandwich panels by Noor et al. (1996). The general approaches adopted for the analysis of sandwich panels, which is a layered structure, use solid plates theories through equivalent one layer approach, such as Mindlin first-order theory, Mindlin (1951) and Wang (1996), Reddy's and other high-order theories, Reddy (1984, 1990, 1997) and recently higher-order theories, see Kant and Mallikarjuna (1989), Senthilnathan et al. (1988) and Kant and Swaminathan (2001). In addition, there are various finite elements approaches: utilizing Reddy's high-order theories, see Meunier and Shenoi (2001) and Nayak et al. (2002); using a "zig-zag" displacement pattern through the thickness of the panel, see Bardell et al. (1997), and using Mindlin plate theory with linearly varying shear stresses and uniform vertical normal stresses through the thickness of the panel which contradicts compatibility within the core, see Lee and Fan (1996). Most of the aforementioned theories and numerical approaches based on finite elements assume that the height of the core remains unchanged, i.e. incompressible, and all of them assume that the boundary conditions for the upper and the lower face sheets are identical at the same edge, which in many cases contradict real plate supports. These assumptions are correct as long as the core is incompressible. However, modern sandwich panels are made of compressible core, foam type, that are usually associated with localized and through the thickness displacements, which the aforementioned theories and models lack to detect. Hence, in order to address these effects an enhanced high-order theory should be used. Analysis using a general finite elements package, such as Ansys or similar, require the use of solid elements for the core as well as for the faces sheets, yields a very fine mesh along with an extremely large model even for very small plates, and demands large computer resources. Hence, an analytical approach that uses a plate approach (2D) for a 3D sandwich panel and takes into account the compressibility of the 3D core, is more then required.

The authors already have used an enhanced high-order theory—the High-order Sandwich Panels Theory (HSAPT). It has successfully been used for various applications in the analysis of sandwich panels, such as: beam analysis, see Frostig et al. (1992), buckling and free vibration, see Frostig and Baruch (1993, 1994), bending and buckling in sandwich plates, see Frostig and Baruch (1996) and Frostig (1998), photoelasticity verification, see Thomsen and Frostig (1997), non-linear behavior, see Sokolinsky and Frostig (2000), free vibration of curved beams, see Bozhevolnaya and Frostig (2001), similitude problems, see Frostig and Simitses (2002), and piezoelectric problems, see Rabinovitch et al. (2003).

The dynamic governing equations, including rotational inertia and the required boundary, conditions are derived explicitly through the Hamilton principle. The mathematical formulation follows the steps of the high-order theory (HSAPT) used for unidirectional panels and plates, see Frostig et al. (1992), Frostig and Baruch (1994, 1996), and Bozhevolnaya and Frostig (2001). The mathematical formulation incorpo-

rates the effects of the flexible core into the equations of motion and the boundary conditions. The sandwich panels are assumed to be elastic, linear with small displacements and consist of a core and two thin plates—the two face sheets, with in-plane and flexural rigidity and negligible shear strain. The core has shear resistance and negligible in-plane and flexural rigidity and its interfaces with the face sheets consist of a full bond and it can resist shear and vertical normal stresses. The external loads are applied at the upper or the lower face sheet only.

Two computational models are proposed; the first one with a formulation that uses the displacements and the shear stresses in the core as its unknowns (mixed formulation), and the second one in which the unknowns are displacements only. The first model follows the principles of HSAPT where the unknowns include also the vertical shear stresses of the core. It yields simple yet accurate governing equations of motion and boundary conditions in terms of stress resultants with a physical meaning. These equations of motion can be verified through equilibrium of a differential element of the sandwich panel with inertial loads. The second model is based on the polynomial displacement distributions of the core through its depth, which are the results of the first computational model, but uses the coefficients of the polynomial distribution as its unknowns. Its principle is similar to the approach used in the high-order shear deformable plate theory by Reddy (1984). This formulation yields higher-order stress resultants that have no physical meaning along with complicated field/governing equations of motion that are derived through variational calculus. The equations of motion in this case cannot be validated by a simple equilibrium approach.

In the first computation model, the inertia forces of the core are transferred to the face sheets and are not incorporated into the governing equations of motion in the core. Hence, the stress and the displacement fields in the core can be described by the closed-form analytical solution of its three-dimensional static governing equations. The analytical solution of these fields consists of a cubic distribution, through the thickness of the core, for the in-plane displacements and a quadratic one for the vertical displacement. The second model is used to investigate the influence of the inconsistency of the first model on the free vibration response. In the second model the dynamic equilibrium equations of the core are fulfilled only in the global sense rather then in the differential one that is used in the first model.

The manuscript outlines the mathematical formulation that includes the derivation of the governing equations of motion along with the associated boundary conditions, and the analytical solution of the displacement and the stress fields of the core in terms of the unknowns in the first computational model. A numerical study of the free vibration of a simply-supported panel with a comparison with the classical and high-order plate theories, along with a parametric study which investigates the effect of the moduli ratio between the core and the face sheets on the lower eigenfrequency, and a comparison between the two models, are presented. Summary and conclusions are presented in the sequel.

2. Mathematical formulation

The mathematical formulation consists of derivation of the governing field equations of motion along with the appropriate boundary conditions for the face sheets and core. They are derived through the Hamilton principle which extremizes the Lagrangian that consists of the kinetic, strain energy and the external work. It reads:

$$\int_{t_1}^{t_2} \delta(-T + U + V)\,\mathrm{d}t = 0 \tag{1}$$

where T is the kinetic energy and U and V are the strain energy and the potential of the external loads respectively, t is the time coordinate between the times t_1 and t_2, and δ denotes the variation operator.

The first variation of the kinetic energy for the sandwich panel reads:

$$\delta T = \int_{V_t} (\rho_t \dot{u}_t \delta \dot{u}_t + \rho_t \dot{v}_t \delta \dot{v}_t + \rho_t \dot{w}_t \delta \dot{w}_t)\,\mathrm{d}v + \int_{V_b} (\rho_b \dot{u}_b \delta \dot{u}_b + \rho_b \dot{v}_b \delta \dot{v}_c + \rho_b \dot{w}_b \delta \dot{w}_b)\,\mathrm{d}v + \int_{V_{\mathrm{core}}} (\rho_c \dot{u}_c \delta \dot{u}_c + \rho_c \dot{v}_c \delta \dot{v}_c + \rho_c \dot{w}_c \delta \dot{w}_c)\,\mathrm{d}v \tag{2}$$

where $\rho_j (j = t, b, c)$ is the density of the upper and lower face sheets and the core, respectively; $\dot{u}_j, \dot{v}_j, \dot{w}_j (j = t, b, c)$ are the velocities in the longitudinal, transverse and vertical direction, respectively, of the various constituents of the sandwich panel; $\dot{f} = \frac{\partial f}{\partial t}$ is the first derivative of the function f with respect to the time coordinate; $V_j (j = t, b, \mathrm{core})$ is the volume of the upper and lower face sheets and core, respectively and $\mathrm{d}v$ is the volume of a differential segment.

The first variation of the strain energy in terms of stresses and strains reads:

$$\delta U = \int_{V_t} (\sigma_{xxt} \delta \varepsilon_{xxt} + \sigma_{yyt} \delta \varepsilon_{yyt} + \tau_{xyt} \delta \gamma_{xyt})\,\mathrm{d}v + \int_{V_b} (\sigma_{xxb} \delta \varepsilon_{xxb} + \sigma_{yyb} \delta \varepsilon_{yyb} + \tau_{xyb} \delta \gamma_{xyb})\,\mathrm{d}v + \int_{V_{\mathrm{core}}} (\tau_{xzc} \delta \gamma_{xzc} + \tau_{yzc} \delta \gamma_{yzc} + \sigma_{zzc} \delta \varepsilon_{zzc})\,\mathrm{d}v \tag{3}$$

where σ_{iij} and ε_{iij} ($i = x$ or y and $j = t, b$) are the longitudinal and transverse normal stresses and strains in the upper and the lower face sheet, respectively; τ_{xyj} and $\gamma_{xyj} (j = t, b)$ are the in-plane shear stress and angle respectively at the various face sheets; τ_{izc} and γ_{izc} ($i = x$ or y) are the vertical shear stresses and shear strains in the core on the longitudinal and transverse faces of the core, and σ_{zzc} and ε_{zzc} are the (vertical) normal stresses and strains in the vertical direction of the core.

The variation of the external work equals:

$$\delta V = -\int_0^a \int_0^b (n_{xt} \delta u_{0t} + n_{xb} \delta u_{0b} + n_{yt} \delta v_{0t} + n_{yb} \delta v_{0b} + q_t \delta w_t + q_b \delta w_b)\,\mathrm{d}x\,\mathrm{d}y \tag{4}$$

where u_{0j}, v_{0j}, and $w_j (j = t, b)$ are the displacements in the longitudinal, transverse and vertical directions, respectively, of the mid-plane of the face sheets; n_{xj} and $n_{yj} (j = t, b)$ are the in-plane external loads in the longitudinal and transverse direction, respectively, of the upper and the lower face sheets and q_t and q_b are the vertical distributed loads exerted on the upper and lower face sheets, respectively. Geometry and sign convention for stresses, displacements, and loads appear in Fig. 1.

The kinematic relations with small linear displacements take the following form:

For the face sheets ($j = t, b$):

$$\begin{aligned} \varepsilon_{xxj} &= \varepsilon_{xx0j} + z_j \chi_{xxj} \\ \varepsilon_{yyj} &= \varepsilon_{yy0j} + z_j \chi_{yyj} \\ \gamma_{xyj} &= \gamma_{xy0j} + z_j \chi_{xyj} \end{aligned} \tag{5}$$

where the mid-plane in-plane strains and curvatures read:

$$\varepsilon_{xx0j} = u_{0j,x}, \quad \varepsilon_{yy0j} = v_{0j,y}, \quad \gamma_{xy0j} = u_{0j,y} + v_{0j,x}$$

$$\chi_{xxj} = -w_{j,xx}, \quad \chi_{yyj} = -w_{j,yy}, \quad \chi_{xyj} = -2w_{j,xy}$$

where ε_{xx0j}, ε_{yy0j} and $\gamma_{xy0j} (j = t, b)$ are the in-plane strains in x and y directions and the in-plane shear angle of the mid-plane of the upper and the lower face sheets, respectively; χ_{xxj}, χ_{yyj} and $\chi_{xyj} (j = t, b)$ are the curvature in the x and y directions and the torsion curvature of the face sheets, respectively; z_j is the vertical

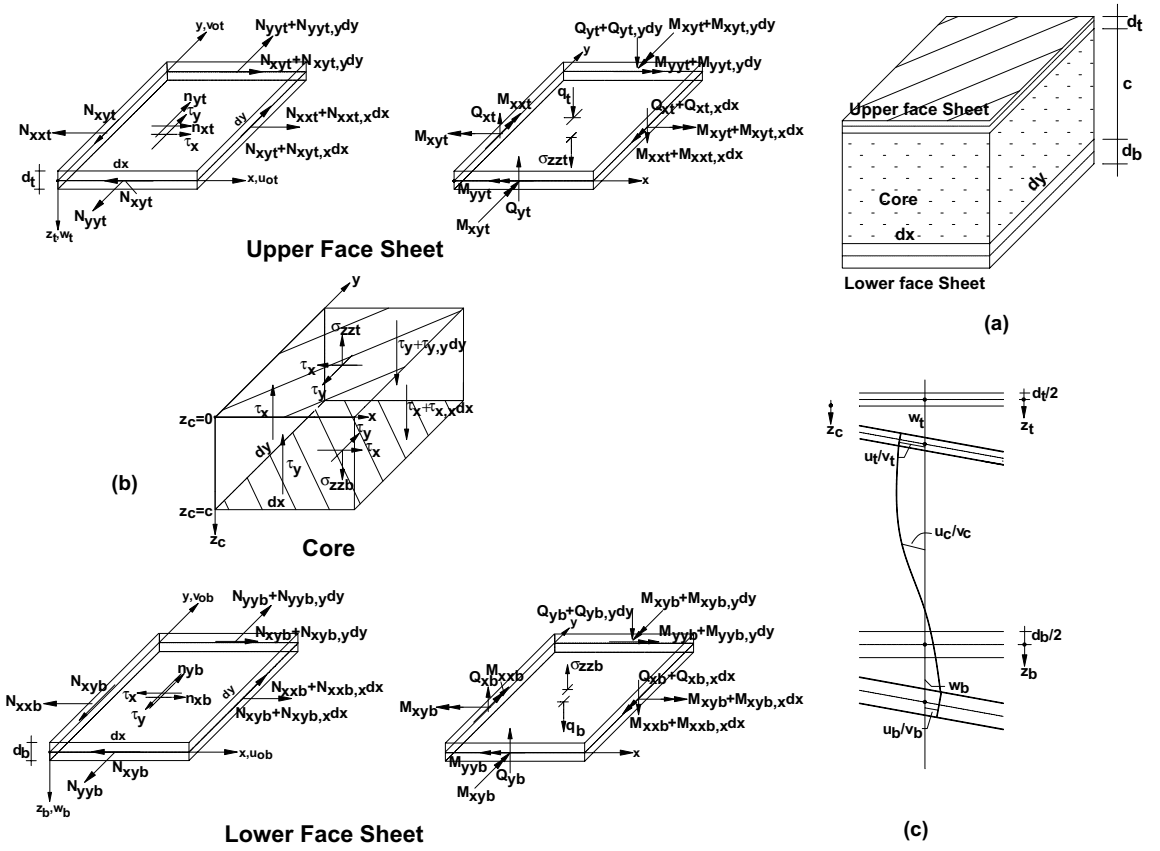

Fig. 1. Geometry, displacement patterns and stress resultants for model I: (a) geometry, (b) stresses, stress resultants and external loads exerted on the face sheets and the core, (c) displacements pattern through the height of the core and the face sheets.

coordinate of each face sheet and is measured downward from the mid-plane of each face sheet (see Fig. 1b), and $(\ ),kl$ denotes a partial derivative with respect to k and l variables.

For the core:

$$\gamma_{xz} = u_{c,z_c} + w_{c,x} \quad \gamma_{yz} = v_{c,z_c} + w_{c,y} \quad \varepsilon_{zz} = w_{c,z_c} \tag{6}$$

where $u_c(x,y,z_c,t)$, $v_c(x,y,z_c,t)$ and $w_c(x,y,z_c,t)$ are the longitudinal, transverse, and vertical deflections of the core, respectively, and z_c is the vertical coordinate of the core, measured downward from the upper interface (see Fig. 1b).

The compatibility conditions at the upper and the lower face–core interface, $(j = t, b)$, read:

$$\begin{aligned} u_c(z = z_{cj}) &= u_{0j} + \tfrac{1}{2}(-1)^k d_j w_{j,x} \\ v_c(z = z_{cj}) &= v_{0j} + \tfrac{1}{2}(-1)^k d_j w_{j,y} \\ w_c(z = z_{cj}) &= w_j \end{aligned} \tag{7}$$

where $k = 0$ when $j = t$ and $k = 1$ when $j = b$; $z_{ct} = 0$ at the upper interface and $z_{cb} = c$ at the lower interface (see Fig. 1b), $u_c(z = z_{cj}), v_c(z = z_{cj})$ and $w_c(z = z_{cj})$ at $(z_{cj} = 0, c)$ are the longitudinal, the transverse, and the vertical deflections, respectively, in the core at the upper and the lower face–core interfaces;

$d_j (j = t, b)$ and c are the thickness of the upper and lower face sheets and the height of the core, respectively, (see Fig. 1a).

The first variation of the kinetic energy assuming homogeneous initial conditions and after integration by parts with respect to the time coordinate, reads:

$$\delta T = -\int_{V_t} (\rho_t \ddot{u}_t \delta u_t + \rho_t \ddot{v}_t \delta v_t + \rho_t \ddot{w}_t \delta w_t)\,\mathrm{d}v - \int_{V_b} (\rho_b \ddot{u}_b \delta u_b + \rho_b \ddot{v}_b \delta v_c + \rho_b \ddot{w}_b \delta w_b)\,\mathrm{d}v - \int_{V_{\text{core}}} (\rho_c \ddot{u}_c \delta u_c + \rho_c \ddot{v}_c \delta v_c + \rho_c \ddot{w}_c \delta w_c)\,\mathrm{d}v \tag{8}$$

where $\ddot{u}_j$, $\ddot{v}_j$, $\ddot{w}_j (j = t, b, c)$ are the accelerations in the longitudinal, transverse and vertical accelerations, respectively, of the various constituents of the sandwich panel, and $\ddot{f} = \frac{\partial^2 f}{\partial t^2}$ denotes the second derivative of the function f with respect to the time coordinate.

The differences between the two computational models are a result of the description of the accelerations and the displacements in the core, (in both models). The two computational models are described next.

2.1. High-order sandwich panel computational model—mixed formulation (model I)

In the first computational model the core is regarded as a medium that transfers its inertial loads to the face sheets, rather than resisting them by itself, in order to prevent wave like behavior in the longitudinal and transverse directions. Hence, the distributions of the accelerations through the depth of the core are assumed to take the shape of the static displacement fields under fully distributed loads, an approach commonly used in many dynamic analyses of ordinary beams, plates and shells, see for example Shames and Dym (1991). The distribution of the static displacements through the depth of the core are in general non-linear, see Eqs. (33), (35) and (36) in Frostig and Baruch (1996), when subjected to a general type of loading, where they depend on the displacements of the upper and the lower face sheets and the vertical shear stresses in the core. The non-linearities in these distributions are associated with significant changes in the vertical shear stresses. However, when fully distributed loads are applied to the face sheets, these non-linearities are small and without a loss of accuracy linear distributions may be used instead. Therefore, the distributions of the acceleration, through the depth of the core, take a linear pattern, as follows:

$$\begin{aligned}
\ddot{u}_c(x,y,z_c,t) &= \ddot{u}_t(x,y,z_t = d_t/2,t)\left(1 - \frac{z_c}{c}\right) + \ddot{u}_b(x,y,z_b = -d_b/2,t)\frac{z_c}{c} \\
\ddot{v}_c(x,y,z_c,t) &= \ddot{v}_t(x,y,z_t = d_t/2,t)\left(1 - \frac{z_c}{c}\right) + \ddot{v}_b(x,y,z_b = -d_b/2,t)\frac{z_c}{c} \\
\ddot{w}_c(x,y,z_c,t) &= \ddot{w}_t(x,y,z_t,t)\left(1 - \frac{z_c}{c}\right) + \ddot{w}_b(x,y,z_b,t)\frac{z_c}{c}
\end{aligned} \tag{9}$$

Notice that this simplification is applied to the kinetic inertia terms only. The second computational model is used to validate the accuracy of this simplification.

The equations of motion and the boundary conditions are derived using Eqs. (1), (3), (4) and (8), with the aid of the kinematic relations, Eqs. (5) and (6), the compatibility conditions, Eq. (7), and the distribution of the acceleration of the core, Eq. (9) together with the stress resultants, see Fig. 1. Hence, after integration by parts, and some algebraic manipulation, the equations of motion read:

For the upper face sheet:

$$\left(\frac{1}{3}u_{0t,tt} + \frac{1}{6}u_{0b,tt} + \frac{1}{12}d_b w_{b,xtt} - \frac{1}{6}d_t w_{t,xtt}\right)M_c - N_{xxt,x} - N_{xyt,y} - \tau_{xzt} + u_{0t,tt}M_t - n_{xt} = 0 \tag{10}$$

$$v_{0t,tt}M_t + \left(\frac{1}{12}d_b w_{b,ytt} + \frac{1}{6}v_{0b,tt} + \frac{1}{3}v_{0t,tt} - \frac{1}{6}d_t w_{t,ytt}\right)M_c - N_{yyt,y} - \tau_{yzt} - N_{xyt,x} - n_{yt} = 0 \tag{11}$$

$$\begin{aligned} w_{t,tt}M_t + \Bigg(& -\frac{1}{12}d_t^2 w_{t,yytt} + \frac{1}{12}u_{0b,xtt}d_t + \frac{1}{24}d_b w_{b,xxtt}d_t + \frac{1}{6}u_{0t,xtt}d_t + \frac{1}{6}w_{b,tt} - \frac{1}{12}d_t^2 w_{t,xxtt} + \frac{1}{6}v_{0t,ytt}d_t \\ & + \frac{1}{24}d_b w_{b,yytt}d_t + \frac{1}{12}v_{0b,ytt}d_t + \frac{1}{3}w_{t,tt}\Bigg)M_c + (-w_{t,xxtt} - w_{t,yytt})I_{mt} - \sigma_{zzt} - 2M_{xyt,xy} - M_{yyt,yy} - q_t \\ & - M_{xxt,xx} - \frac{1}{2}\tau_{yzt,y}d_t - \frac{1}{2}\tau_{xzt,x}d_t = 0 \end{aligned} \tag{12}$$

For the lower face sheet:

$$\left(\frac{1}{3}u_{0b,tt} - \frac{1}{12}d_t w_{t,xtt} + \frac{1}{6}d_b w_{b,xtt} + \frac{1}{6}u_{0t,tt}\right)M_c + u_{0b,tt}M_b - n_{xb} + \tau_{xzb} - N_{xxb,x} - N_{xyb,y} = 0 \tag{13}$$

$$\left(\frac{1}{6}v_{0t,tt} + \frac{1}{3}v_{0b,tt} + \frac{1}{6}d_b w_{b,ytt} - \frac{1}{12}d_t w_{t,ytt}\right)M_c + v_{0b,tt}M_b + \tau_{yzb} - N_{yyb,y} - n_{yb} - N_{xyb,x} = 0 \tag{14}$$

$$\begin{aligned} \Bigg(& -\frac{1}{12}v_{0t,ytt}d_b + \frac{1}{6}w_{t,tt} + \frac{1}{24}d_t w_{t,yytt}d_b - \frac{1}{12}d_b^2 w_{b,yytt} + \frac{1}{3}w_{b,tt} - \frac{1}{12}u_{0t,xtt}d_b - \frac{1}{6}u_{0b,xtt}d_b - \frac{1}{12}d_b^2 w_{b,xxtt} \\ & + \frac{1}{24}d_t w_{t,xxtt}d_b - \frac{1}{6}v_{0b,ytt}d_b\Bigg)M_c + w_{b,tt}M_b + (-w_{b,yytt} - w_{b,xxtt})I_{mb} - 2M_{xyb,xy} - M_{yyb,yy} - \frac{1}{2}\tau_{yzb,y}d_b \\ & - q_b - \frac{1}{2}\tau_{xzb,x}d_b - M_{xxb,xx} + \sigma_{zzb} = 0 \end{aligned} \tag{15}$$

where N_{xxj}, N_{yyj} *and* $N_{xyj}(j = t, b)$ are the normal stress resultants in the longitudinal and the transverse directions, and the in-plane shear stress resultant, respectively both, at the upper and the lower face sheets; M_{xxj}, M_{yyj} and $M_{xyj}(j = t, b)$ are the bending moment in the longitudinal and the transverse directions and the torsion moment, respectively, at various face sheets; τ_{xzj}, τ_{yzj} and $\sigma_{zzj}(j = t, b)$ are the shear stresses in the longitudinal and transverse directions and the vertical normal stresses of the core, respectively both, at the upper and the lower face–core interfaces $M_j, I_{mj}(j = t, b)$ are the mass and the rotary inertia per area unit, respectively of the upper and the lower face sheets, M_c is the mass per area unit of core and $(\ )_{,ijtt}$ denoting partial derivative with respect to i and j and t, where the indices refer to the coordinates of the panel and the time coordinate. For sign convention see Fig. 1b.

For the core:

$$\begin{aligned} & -\tau_{xzc,z_c} = 0, -\tau_{yzc,z_c} = 0 \\ & -\tau_{xzc,x} - \sigma_{zzc,z_c} - \tau_{yzc,y} = 0 \end{aligned} \tag{16}$$

Notice, that the field/equilibrium equations of the core are fulfilled in the differential sense rather than the global one (see dynamic equilibrium equations of model II herein). The shear stresses, τ_{xzc} and τ_{yzc}, are uniform through the height of the core and are functions of the x and y coordinates and time only. Thus

$$\tau_{xzc}(x, y, z_c, t) = \tau_x(x, y, t), \quad \tau_{yzc}(x, y, z_c, t) = \tau_y(x, y, t) \tag{17}$$

Therefore, the shear stresses at the upper and the lower face–core interfaces in the various directions read: $\tau_{xzt} = \tau_{xzb} = \tau_x$ and $\tau_{yzt} = \tau_{yzb} = \tau_y$ (see Eqs. (10)–(15)). Notice, that although the inertia loads of the core exist, their contribution has been transferred to the upper and the lower faces. Hence its equations of motion equal those of the static ones, see Frostig and Baruch (1996).

The boundary conditions at the edges of the panel for each face sheet ($j = t, b$) and the core, read:
For the upper and the lower face sheets, ($j = t, b$), at $x = 0$ or a:

$$\lambda_{bc}N_{xxj} - N_{xx,\text{ext}} = 0 \quad \text{or} \quad u_{0j} = u_{0j,\text{ext}} \tag{18}$$

$$\lambda_{bc}N_{xyj} - N_{xy,\text{ext}} = 0 \quad \text{or} \quad v_{0j} = v_{0j,\text{ext}} \tag{19}$$

$$-\lambda_{bc}M_{xxj} - M_{xx,\text{ext}} = 0 \quad \text{or} \quad w_{j,x} = \theta_{x,\text{ext}} \tag{20}$$

$$\lambda_{bc}\left(\left(-\frac{1}{6}u_{0t,tt}d_t - \frac{1}{24}d_b w_{b,xtt}d_t - \frac{1}{12}u_{0b,tt}d_t + \frac{1}{12}d_t^2 w_{t,xtt}\right)M_c + 2M_{xyt,y} + w_{t,xtt}I_{mt} + \frac{1}{2}\tau_x d_t + M_{xxt,x}\right) = V_{xt,\text{ext}} \quad \text{or} \quad w_t = w_{t,\text{ext}} \tag{21}$$

$$\lambda_{bc}\left(\left(\frac{1}{6}u_{0b,tt}d_b + \frac{1}{12}d_b^2 w_{b,xtt} + \frac{1}{12}u_{0t,tt}d_b - \frac{1}{24}d_t w_{t,xtt}d_b\right)M_c + 2M_{xyb,y} + w_{b,xtt}I_{mb} + \frac{1}{2}\tau_x d_b + M_{xxb,x}\right) = V_{xb,\text{ext}} \quad \text{or} \quad w_b = w_{b,\text{ext}} \tag{22}$$

For the upper and the lower face sheets, ($j = t, b$), at $y = 0$ or b:

$$\lambda_{bc}N_{xyj} - N_{xy,\text{ext}} = 0 \quad \text{or} \quad u_{0j} = u_{0j,\text{ext}} \tag{23}$$

$$\lambda_{bc}N_{yyj} - N_{yy,\text{ext}} = 0 \quad \text{or} \quad v_{0j} = v_{0j,\text{ext}} \tag{24}$$

$$-\lambda_{bc}M_{yyj} - M_{yy,\text{ext}} = 0 \quad \text{or} \quad w_{j,y} = \theta_{y,\text{ext}} \tag{25}$$

$$\lambda_{bc}\left(\left(-\frac{1}{12}v_{0b,tt}d_t - \frac{1}{6}v_{0t,tt}d_t - \frac{1}{24}d_b w_{b,ytt}d_t + \frac{1}{12}d_t^2 w_{t,ytt}\right)M_c + \frac{1}{2}\tau_y d_t + w_{t,ytt}I_{mt} + M_{yyt,y} + 2M_{xyt,x}\right) = V_{yt,\text{ext}} \quad \text{or} \quad w_t = w_{t,\text{ext}} \tag{26}$$

$$\lambda_{bc}\left(\left(-\frac{1}{24}d_t w_{t,ytt}d_b + \frac{1}{6}v_{0b,tt}d_b + \frac{1}{12}d_b^2 w_{b,ytt} + \frac{1}{12}v_{0t,tt}d_b\right)M_c + M_{yyb,y} + \frac{1}{2}\tau_y d_b + 2M_{xyb,x} + w_{b,ytt}I_{mb}\right) = V_{yb,\text{ext}} \quad \text{or} \quad w_b = w_{b,\text{ext}} \tag{27}$$

For the upper and the lower face sheets, ($j = t, b$) at the four corners of panel ($x = 0$ *or* a and $y = 0$ *or* b):

$$M_{xyj} = 0 \quad \text{or} \quad w_j = 0 \tag{28}$$

where $N_{lkj,\text{ext}}, M_{lkj,\text{ext}}$ and $V_{(l \text{ or } k)j,\text{ext}}$ ($l, k = x, y$ and $j = t, b$) are the external in-plane longitudinal and shear loads, the bending moments and the vertical external loads exerted at the edges of the upper and the lower face sheets at $x = 0$ *or* a, and at $y = 0$ *or* b, respectively, and $\lambda_{bc} = 1$ at $x = a$ *or* $y = b$ and $\lambda_{bc} = -1$ at $x = y = 0$. Notice that the inertia terms appear also in the boundary conditions.

At any point through the height of the core, $z_c = z$, the boundary conditions at the edges read:

$$\begin{aligned} &\tau_x(x = 0, a) = 0 \quad \text{or} \quad w_c(x = 0, a, z_c) = w_{c,\text{ext}}(z_c) \\ &\tau_y(y = 0, b) = 0 \quad \text{or} \quad w_c(y = 0, b, z_c) = w_{c,\text{ext}}(z_c) \end{aligned} \tag{29}$$

where $w_{c,\text{ext}}(z_c)$ is the external induced displacement through the depth of the core.

The constitutive relations for each face sheet using laminated composite materials with a general lay-up yield the following stress resultant—displacement relations ($j = t, b$):

$$
\begin{aligned}
N_{xxj} &= A11_j\varepsilon_{0xxj} + A12_j\varepsilon_{0yyj} + A16_j\gamma_{0xyj} + B11_j\chi_{xxj} + B12_j\chi_{yyj} + B16_j\chi_{xyj}\\
N_{yyj} &= A12_j\varepsilon_{0xxj} + A22_j\varepsilon_{0yyj} + A26_j\gamma_{0xyj} + B12_j\chi_{xxj} + B22_j\chi_{yyj} + B26_j\chi_{xyj}\\
N_{xyj} &= A16_j\varepsilon_{0xxj} + A26_j\varepsilon_{0yyj} + A66_j\gamma_{0xyj} + B16_j\chi_{xxj} + B26_j\chi_{yyj} + B66_j\chi_{xyj}\\
M_{xxj} &= B11_j\varepsilon_{0xxj} + B12_j\varepsilon_{0yyj} + B16_j\gamma_{0xyj} + D11_j\chi_{xxj} + D12_j\chi_{yyj} + D16_j\chi_{xyj}\\
M_{yyj} &= B12_j\varepsilon_{0xxj} + B22_j\varepsilon_{0yyj} + B26_j\gamma_{0xyj} + D12_j\chi_{xxj} + D22_j\chi_{yyj} + D26_j\chi_{xyj}\\
M_{xyj} &= B16_j\varepsilon_{0xxj} + B26_j\varepsilon_{0yyj} + B66_j\gamma_{0xyj} + D16_j\chi_{xxj} + D26_j\chi_{yyj} + D66_j\chi_{xyj}
\end{aligned}
\tag{30}
$$

where Amn_j, Bmn_j, and Dmn_j ($m,n = 1,2,6$ and $j = t,b$) are the reduced in-plane and flexural rigidities with respect to the mid-plane of each face sheet, see Whitney (1987) and ε_{0ikj} and χ_{ikj} ($i = k = x,y$ and $j = t,b$), are the mid-plane strains and curvature, respectively, of the upper and the lower face sheets, see Eq. (5).

The constitutive relations for the core with negligible in-plane stresses and orthotropic in shear, equal:

$$
\varepsilon_{zzc} = \frac{\sigma_{zzc}}{E_{zc}}, \quad \gamma_{xzc} = \frac{\tau_x}{G_{xc}}, \quad \gamma_{yzc} = \frac{\tau_y}{G_{yc}} \tag{31}
$$

where E_{zc} is the modulus of elasticity of the core in the vertical direction, and G_{xc} and G_{yc} are the vertical shear moduli on the x and y faces of the core.

The core stress and displacements fields must first be determined in order to describe the equations of motion in terms of the displacements and the shear stresses. The core fields, in this model, equal those of the static case, see Frostig and Baruch (1996) and Frostig (1998), since the inertia loads of the core have been transferred to the face sheets, see Eq. (16). The stresses and the displacements fields for the orthotropic core in shear can be found in Frostig (1998) and are presented here for completeness.

The vertical normal stresses within the core and at the upper and the lower face–core interfaces equal:

$$
\begin{aligned}
\sigma_{zzc} &= \left(-\frac{w_t}{c} + \frac{w_b}{c}\right)E_{zc} + \left(-z_c + \frac{c}{2}\right)\tau_{x,x} + \left(-z_c + \frac{c}{2}\right)\tau_{y,y}\\
\sigma_{zzt} &= \left(-\frac{w_t}{c} + \frac{w_b}{c}\right)E_{zc} + \tfrac{1}{2}\tau_{x,x}c + \tfrac{1}{2}\tau_{y,y}c\\
\sigma_{zzb} &= \left(-\frac{w_t}{c} + \frac{w_b}{c}\right)E_{zc} - \tfrac{1}{2}\tau_{x,x}c - \tfrac{1}{2}\tau_{y,y}c
\end{aligned}
\tag{32}
$$

The displacement distributions in the longitudinal, transverse and the vertical directions read:

$$
\begin{aligned}
u_c &= \left(\frac{1}{6}\frac{z_c^3}{E_{zc}} - \frac{1}{4}\frac{cz_c^2}{E_{zc}}\right)\tau_{y,xy} + \frac{\tau_x z_c}{G_{xc}} + \left(\frac{1}{6}\frac{z_c^3}{E_{zc}} - \frac{1}{4}\frac{cz_c^2}{E_{zc}}\right)\tau_{x,xx} + \left(-z_c + \frac{1}{2}\frac{z_c^2}{c} - \frac{1}{2}d_t\right)w_{t,x}\\
&\quad + u_{0t} - \frac{1}{2}\frac{w_{b,x}z_c^2}{c}\\
v_c &= \left(\frac{1}{6}\frac{z_c^3}{E_{zc}} - \frac{1}{4}\frac{cz_c^2}{E_{zc}}\right)\tau_{x,xy} + \left(-z_c + \frac{1}{2}\frac{z_c^2}{c} - \frac{1}{2}d_t\right)w_{t,y} + \frac{\tau_y z_c}{G_{yc}} + \left(\frac{1}{6}\frac{z_c^3}{E_{zc}} - \frac{1}{4}\frac{cz_c^2}{E_{zc}}\right)\tau_{y,yy}\\
&\quad + v_{0t} - \frac{1}{2}\frac{w_{b,y}z_c^2}{c}\\
w_c &= \left(-\frac{1}{2}\frac{z_c^2}{E_{zc}} + \frac{1}{2}\frac{cz_c}{E_{zc}}\right)\tau_{x,x} + \left(-\frac{1}{2}\frac{z_c^2}{E_{zc}} + \frac{1}{2}\frac{cz_c}{E_{zc}}\right)\tau_{y,y} + \left(-\frac{z_c}{c} + 1\right)w_t + \frac{w_b z_c}{c}
\end{aligned}
\tag{33}
$$

The stress and displacements fields within the core have been determined through: the closed-form solution of the equilibrium equations, see Eq. (16); the compatibility requirement of the vertical displacements at the upper and the lower face–core interface, see third equation in Eq. (7); and the compatibility requirements at the upper face–core interface in the longitudinal and the transverse direction, see first two equations in

Eq. (7). The additional two compatibility conditions in the longitudinal and transverse directions, at the lower face sheet–core interface, are part of the governing dynamic equations, see Eqs. (40) and (41) ahead.

Notice that the displacement patterns in the various directions, through the depth of the core are in general non-linear. The in-plane displacements take cubic polynomial distributions and the vertical displacement has a quadratic one. However, in the case of fully distributed loads these patterns become linear and the contributions of the vertical shear stresses in the core are almost null.

The governing equations of motion are formulated in terms of the following eight unknowns: the in-plane displacements of the mid-plane of the face sheets in the x direction and y direction, the vertical deflections of the upper and the lower face sheets and the vertical shear stresses in the core on the x and y faces. The first six equations are determined through substitution of the constitutive relations, see Eq. (30), in the equations of motion of the face sheets, Eqs. (10)–(15) along with Eq. (32). The additional two equations are derived using the in-plane displacement distributions of the core in x and y directions, Eq. (33), and the compatibility requirements at the lower face–core interface in the x and y direction, Eq. (7). Hence, the governing equations of motion read:

$$\left(\frac{1}{3}u_{0t,tt}+\frac{1}{6}u_{0b,tt}+\frac{1}{12}d_b w_{b,xtt}-\frac{1}{6}d_t w_{t,xtt}\right)M_c-\tau_x+u_{0t,tt}M_t+B11_t w_{t,xxx}-n_{xt}-A16_t v_{0t,yy}$$
$$+(-A66_t-A12_t)v_{0t,xy}-A16_t v_{0t,xx}-2A16_t u_{0t,xy}-A11_t u_{0t,xx}-A66_t u_{0t,yy}+(B12_t+2B66_t)w_{t,yyx}$$
$$+B26_t w_{t,yyy}+3B16_t w_{t,xxy}=0 \tag{34}$$

$$\left(\frac{1}{12}d_b w_{b,ytt}+\frac{1}{6}v_{0b,tt}+\frac{1}{3}v_{0t,tt}-\frac{1}{6}d_t w_{t,ytt}\right)M_c-\tau_y+v_{0t,tt}M_t-A66_t v_{0t,xx}+(-A66_t-A12_t)u_{0t,xy}$$
$$-A22_t v_{0t,yy}+(-A26_t-A16_t)v_{0t,xy}+3B26_t w_{t,yyx}+B16_t w_{t,xxx}-A16_t u_{0t,xx}-A26_t u_{0t,yy}-n_{yt}$$
$$+B22_t w_{t,yyy}+(B12_t+2B66_t)w_{t,xxy}=0 \tag{35}$$

$$\left(-\frac{c}{2}-\frac{1}{2}d_t\right)\tau_{x,x}+\left(-\frac{c}{2}-\frac{1}{2}d_t\right)\tau_{y,y}+\left(\frac{w_t}{c}-\frac{w_b}{c}\right)E_{zc}-B11_t u_{0t,xxx}+\left(\frac{1}{12}v_{0b,ytt}d_t+\frac{1}{6}u_{0t,xtt}d_t\right.$$
$$-\frac{1}{12}d_t^2 w_{t,yytt}+\frac{1}{6}v_{0t,ytt}d_t-\frac{1}{12}d_t^2 w_{t,xxtt}+\frac{1}{3}w_{t,tt}+\frac{1}{12}u_{0b,xtt}d_t+\frac{1}{6}w_{b,tt}+\frac{1}{24}d_b w_{b,yytt}d_t$$
$$\left.+\frac{1}{24}d_b w_{b,xxtt}d_t\right)M_c+(-w_{t,xxtt}-w_{t,yytt})I_{mt}+(-2B66_t-B12_t)v_{0t,xxy}-B26_t u_{0t,yyy}+4D16_t w_{t,xxxy}$$
$$+D11_t w_{t,xxxx}+4D26_t w_{t,xyyy}+(4D66_t+2D12_t)w_{t,xxyy}-q_t+(-2B66_t-B12_t)u_{0t,xyy}+D22_t w_{t,yyyy}$$
$$+w_{t,tt}M_t-B22_t v_{0t,yyy}-3B16_t u_{0t,xxy}+(-B26_t-2B16_t)v_{0t,xyy}-B16_t v_{0t,xxx}=0 \tag{36}$$

$$\left(\frac{1}{3}u_{0b,tt}+\frac{1}{6}u_{0t,tt}+\frac{1}{6}d_b w_{b,xtt}-\frac{1}{12}d_t w_{t,xtt}\right)M_c+\tau_x-n_{xb}+M_b u_{0b,tt}+(-A12_b-A66_b)v_{0b,xy}$$
$$-A66_b u_{0b,yy}+B11_b w_{b,xxx}+B26_b w_{b,yyy}-2A16_b u_{0b,xy}-A16_b v_{0b,xx}-A16_b v_{0b,yy}-A11_b u_{0b,xx}$$
$$+(2B66_b+B12_b)w_{b,yyx}+3B16_b w_{b,xxy}=0 \tag{37}$$

$$\left(\frac{1}{6}v_{0t,tt}+\frac{1}{3}v_{0b,tt}+\frac{1}{6}d_b w_{b,ytt}-\frac{1}{12}d_t w_{t,ytt}\right)M_c+\tau_y+B16_b w_{b,xxx}+v_{0b,tt}M_b-n_{yb}-A26_b u_{0b,yy}$$
$$-A22_b v_{0b,yy}+B22_b w_{b,yyy}+(-A16_b-A26_b)v_{0b,xy}-A66_b v_{0b,xx}+(2B66_b+B12_b)w_{b,xxy}$$
$$-A16_b u_{0b,xx}+(-A12_b-A66_b)u_{0b,xy}+3B26_b w_{b,yyx}=0 \tag{38}$$

$$\left(-\frac{w_t}{c}+\frac{w_b}{c}\right)E_{zc}+\left(-\frac{1}{12}v_{0t,ytt}d_b-\frac{1}{12}d_b^2w_{b,xxtt}-\frac{1}{6}v_{0b,ytt}d_b-\frac{1}{12}u_{0t,xtt}d_b-\frac{1}{6}u_{0b,xtt}d_b+\frac{1}{6}w_{t,tt}\right.$$
$$\left.-\frac{1}{12}d_b^2w_{b,yytt}+\frac{1}{3}w_{b,tt}+\frac{1}{24}d_tw_{t,yytt}d_b+\frac{1}{24}d_tw_{t,xxtt}d_b\right)M_c+\left(-\frac{c}{2}-\frac{1}{2}d_b\right)\tau_{x,x}+\left(-\frac{c}{2}-\frac{1}{2}d_b\right)\tau_{y,y}$$
$$+D22_bw_{b,yyyy}-B22_bv_{0b,yyy}-3B16_bu_{0b,xxy}+M_bw_{b,tt}-B11_bu_{0b,xxx}-I_{mb}w_{b,xxtt}+D11_bw_{b,xxxx}-q_b$$
$$+(-2B16_b-B26_b)v_{0b,xyy}+(-2B66_b-B12_b)v_{0b,xxy}+4D16_bw_{b,xxxy}+(-2B66_b-B12_b)u_{0b,xyy}$$
$$+(2D12_b+4D66_b)w_{b,xxyy}-I_{mb}w_{b,yytt}-B26_bu_{0b,yyy}+4D26_bw_{b,xyyy}-B16_bv_{0b,xxx}=0 \tag{39}$$

$$\left(\frac{c}{2}+\frac{1}{2}d_t\right)w_{t,y}+\left(\frac{c}{2}+\frac{1}{2}d_b\right)w_{b,y}-v_{0t}+\frac{1}{12}\frac{c^3\tau_{x,xy}}{E_{zc}}-\frac{\tau_yc}{G_{yc}}+\frac{1}{12}\frac{c^3\tau_{y,yy}}{E_{zc}}+v_{0b}=0 \tag{40}$$

$$\left(\frac{c}{2}+\frac{1}{2}d_t\right)w_{t,x}+\left(\frac{c}{2}+\frac{1}{2}d_b\right)w_{b,x}-\frac{\tau_xc}{G_{xc}}+\frac{1}{12}\frac{c^3\tau_{x,xx}}{E_{zc}}+u_{0b}-u_{0t}+\frac{1}{12}\frac{c^3\tau_{y,xy}}{E_{zc}}=0 \tag{41}$$

The governing equations of motion consist of a set of partial differential equations in three dimensions- two in space, and one in time, of the order of twenty with six equations of the second order and two equations of the fourth order, which also coincide with the number of boundary conditions, see Eqs. (18)–(29). In the case of a harmonic excitation the original set is replaced by a set of PDE's in two dimensions only. The solution of this set can be achieved numerically for a general type of boundary condition and external dynamic loads, or analytically, for the particular case of a simply-supported plate.

2.2. Free vibration of a simply-supported panel—model I

The free vibrations of a simply-supported sandwich panel are presented next. The edges of the upper and the lower face sheets are simply-supported and the vertical displacements of the core through its depth, at the edges are prevented. The face sheets consist of a specially orthotropic construction, with unsymmetrical lay-up, where the $Ai6_j$, $Bi6_j$ and the $Di6_j (i = 1, 2 \text{ and } j = t, b)$ are null. In such a case a closed-form solution exists and it consists of a Fourier series in two-dimensions along with a harmonic time function that fully satisfies the boundary conditions of a simply-supported panel. However, since each coefficients of the Fourier series are independent, a one-term solution exists.

The series solution reads $(j = t, b)$:

$$u_{0j}(x,y,t)=\left(\sum_{n=1}^{N}\left(\sum_{m=1}^{M}C_{u_{0j}}^{mn}\cos(\alpha_mx)\sin(\beta_ny)\right)\right)e^{(\omega tI)}$$
$$v_{0j}(x,y,t)=\left(\sum_{n=1}^{N}\left(\sum_{m=1}^{M}C_{v_{0j}}^{mn}\sin(\alpha_mx)\cos(\beta_ny)\right)\right)e^{(\omega tI)}$$
$$w_j(x,y,t)=\left(\sum_{n=1}^{N}\left(\sum_{m=1}^{M}C_{w_j}^{mn}\sin(\alpha_mx)\sin(\beta_ny)\right)\right)e^{(\omega tI)} \tag{42}$$
$$\tau_x(x,y,t)=\left(\sum_{n=1}^{N}\left(\sum_{m=1}^{M}C_{\tau_x}^{mn}\cos(\alpha_mx)\sin(\beta_ny)\right)\right)e^{(\omega tI)}$$
$$\tau_y(x,y,t)=\left(\sum_{n=1}^{N}\left(\sum_{m=1}^{M}C_{\tau_y}^{mn}\sin(\alpha_mx)\cos(\beta_ny)\right)\right)e^{(\omega tI)}$$

where M and N are the number of terms in the truncated series in longitudinal and transverse directions, respectively; $C_{f_j}^{mn}$ ($f_j = u_{0t}, v_{0t}, w_t, u_{0b}, v_{0b}, w_b, \tau_x$ and τ_y) are the constants of the series solution; $\alpha_m = m\pi/a$ and $\beta_n = n\pi/b$ where m and n are the wave numbers, a and b are the length and width of the panel, I is the complex notation and ω is the eigenfrequency of the panel.

The solution is determined through substitution of a general term of the series, Eq. (42), into the governing equations, Eqs. (34)–(41) which yields a set of homogeneous algebraic equations for each m and n term, instead of the set of partial differential equations. Thus, the solution of the PDE's is replaced by an eigenvalue problem, with a mass and a stiffness matrix, where the square of the eigenfrequency equals to the eigenvalue and the series constants for each m and n are the corresponding eigenvectors. The corresponding dimension of the stiffness matrix is 8, and that of the mass matrix is only 6. It happens since the last two equations of motion, see Eqs. (40) and (41), that describe the compatibility conditions in the longitudinal and the transverse direction at the lower face–core interface, do not contain any inertia terms. Hence, the stiffness matrix can be condensed into a dimension of 6 that of the mass matrix by removing C_{τ_x} and C_{τ_y}. Thus, the eigenvalue problem yields only six eigenfrequencies for specified values of m and n.

2.3. High-order sandwich panel computational model—displacements formulation (model II)

The second computational model is used to investigate the accuracy of the results of the first model due to the differences between the distributions of the accelerations through the depth of the core, see Eq. (9) and its displacement fields, see Eq. (33). The advantage of this formulation is that the dynamic loads are directly included in the equations of motion of the core and not through the interaction with the upper and the lower face sheets, but at the cost of using higher bending moments and shear stress resultants that lack any physical meaning. The formulation follows the same steps as the previous model, using the same basic equations, Eqs. (1)–(8), but here the unknowns are the displacements of the face sheets and the core. In order to achieve this goal, the displacements fields of the core are assumed a priori, using the distribution of the displacement fields that have been found in the previous model, see Eq. (33), but where the coefficients of the polynomial distribution are the unknowns. Thus, the displacements fields for the core take a cubic pattern for the in-plane displacements and a quadratic one for the vertical ones, and they read:

$$\begin{aligned} u_c(x,y,z_c,t) &= u_0(x,y,t) + u_1(x,y,t)z_c + u_2(x,y,t)z_c^2 + u_3(x,y,t)z_c^3 \\ v_c(x,y,z_c,t) &= v_0(x,y,t) + v_1(x,y,t)z_c + v_2(x,y,t)z_c^2 + v_3(x,y,t)z_c^3 \\ w_c(x,y,z_c,t) &= w_0(x,y,t) + w_1(x,y,t)z_c + w_2(x,y,t)z_c^2 \end{aligned} \tag{43}$$

where u_k and $v_k (k = 0,1,2,3)$ are the unknowns of the in-plane displacements of the core and $w_l (l = 0,1,2)$ are the unknowns of its vertical displacements, respectively. It is assumed that the accelerations and velocities in the core have the same distributions. The compatibility conditions at the upper and the lower face–core interfaces, see Eq. (7), are fulfilled using six Lagrange multipliers, see Fig. 2. Thus, the variation of the strain energy, see Eq. (3), reads:

$$\begin{aligned} \delta U = &\int_{V_t} (\sigma_{xxt}\delta\varepsilon_{xxt} + \sigma_{yyt}\delta\varepsilon_{yyt} + \tau_{xyt}\delta\gamma_{xyt})\,\mathrm{d}v + \int_{V_b} (\sigma_{xxb}\delta\varepsilon_{xxb} + \sigma_{yyb}\delta\varepsilon_{yyb} + \tau_{xyb}\delta\gamma_{xyb})\,\mathrm{d}v \\ &+ \int_{V_{\text{core}}} (\tau_{xzc}\delta\gamma_{xzc} + \tau_{yzc}\delta\gamma_{yzc} + \sigma_{zzc}\delta\varepsilon_{zzc})\,\mathrm{d}v + \delta\Bigg[\int_0^a\int_0^b \lambda_{xt}(u_t(z_t = d_t/2) - u_c(z_c = -c/2)) \\ &+ \lambda_{yt}(v_t(z_t = d_t/2) - v_c(z_c = -c/2)) + \lambda_{zt}(w_t - w_c(z_c = -c/2) + \lambda_{xb}(u_c(z_c = c/2) \\ &- u_b(z_b = -d_b/2)) + \lambda_{yb}(v_c(z_c = c/2) - v_b(z_b = -d_b/2)) + \lambda_{zb}(w_c(z_c = c/2) - w_b))\,\mathrm{d}x\,\mathrm{d}y\Bigg] \end{aligned} \tag{44}$$

where z_c here, is measured downwards from mid-height of core, see Fig. 2.

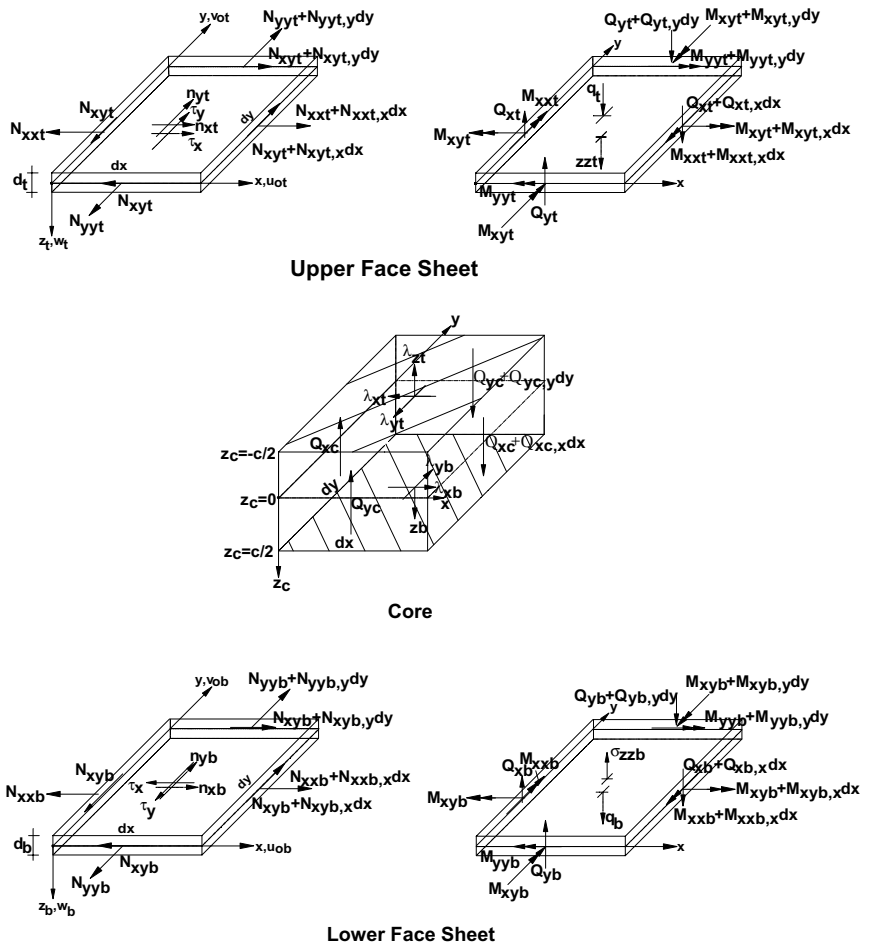

Fig. 2. Stress resultants and external loads in model II.

The equations of motion and the boundary conditions of this computational model are derived using Eqs. (1), (44), (4) and (8), with the aid of the kinematic relations, Eqs. (5) and (6), the compatibility conditions, Eq. (7), along with the Lagrange multipliers and the distribution of the acceleration of the core following Eq. (43), together with the stress resultants that appear in Fig. 2, and high-order stress resultants. Hence, after integration by parts and some algebraic manipulation, the equations of motion and the compatibility equations read:

$$u_{0t,tt}M_t - N_{xxt,x} - \lambda_{xt} - n_{xt} - N_{xyt,y} = 0 \tag{45}$$

$$-\lambda_{yt} - N_{xyt,x} - n_{yt} - N_{yyt,y} + v_{0t,tt}M_t = 0 \tag{46}$$

$$w_{t,tt}M_t + (-w_{t,xxtt} - w_{t,yytt})I_{mt} - M_{xxt,xx} + \frac{1}{2}\lambda_{yt,y}d_t - M_{yyt,yy} - 2M_{xyt,xy} - \lambda_{zt} + \frac{1}{2}\lambda_{xt,x}d_t - q_t = 0 \tag{47}$$

$$u_{0b,tt}M_b + \lambda_{xb} - N_{xyb,y} - N_{xxb,x} - n_{xb} = 0 \tag{48}$$

$$v_{0b,tt}M_b - N_{xyb,x} - N_{yyb,y} + \lambda_{yb} - n_{yb} = 0 \tag{49}$$

$$w_{b,tt}M_b + (-w_{b,xxtt} - w_{b,yytt})I_{mb} - M_{yyb,yy} + \frac{1}{2}\lambda_{xb,x}d_b - q_b + \frac{1}{2}\lambda_{yb,y}d_b + \lambda_{zb} - 2M_{xyb,xy} - M_{xxb,xx} = 0 \tag{50}$$

$$\left(\frac{1}{12}c^2u_{2,tt} + u_{0,tt}\right)M_c + \lambda_{xt} - \lambda_{xb} = 0 \tag{51}$$

$$\left(\frac{1}{80}c^4u_{3,tt} + \frac{1}{12}c^2u_{1,tt}\right)M_c - \frac{1}{2}c\lambda_{xt} - \frac{1}{2}\lambda_{xb}c + Q_{xc} = 0 \tag{52}$$

$$\left(\frac{1}{80}c^4u_{2,tt} + \frac{1}{12}c^2u_{0,tt}\right)M_c + \frac{1}{4}\lambda_{xt}c^2 + 2M_{Q1xc} - \frac{1}{4}\lambda_{xb}c^2 = 0 \tag{53}$$

$$\left(\frac{1}{448}c^6u_{3,tt} + \frac{1}{80}c^4u_{1,tt}\right)M_c - \frac{1}{8}\lambda_{xb}c^3 - \frac{1}{8}\lambda_{xt}c^3 + 3M_{Q2xc} = 0 \tag{54}$$

$$\left(v_{0,tt} + \frac{1}{12}c^2v_{2,tt}\right)M_c + \lambda_{yt} - \lambda_{yb} = 0 \tag{55}$$

$$\left(\frac{1}{80}c^4v_{3,tt} + \frac{1}{12}c^2v_{1,tt}\right)M_c + Q_{yc} - \frac{1}{2}\lambda_{yt}c - \frac{1}{2}\lambda_{yb}c = 0 \tag{56}$$

$$\left(\frac{1}{80}c^4v_{2,tt} + \frac{1}{12}c^2v_{0,tt}\right)M_c + 2M_{Q1yc} - \frac{1}{4}\lambda_{yb}c^2 + \frac{1}{4}c^2\lambda_{yt} = 0 \tag{57}$$

$$\left(\frac{1}{80}c^4v_{1,tt} + \frac{1}{448}c^6v_{3,tt}\right)M_c + 3M_{Q2yc} - \frac{1}{8}\lambda_{yt}c^3 - \frac{1}{8}\lambda_{yb}c^3 = 0 \tag{58}$$

$$\left(w_{0,tt} + \frac{1}{12}c^2w_{2,tt}\right)M_c - Q_{xc,x} - Q_{yc,y} + \lambda_{zt} - \lambda_{zb} = 0 \tag{59}$$

$$\frac{1}{12}M_cc^2w_{1,tt} - M_{Q1yc,y} - \frac{1}{2}\lambda_{zt}c + R_{zc} - \frac{1}{2}\lambda_{zb}c - M_{Q1xc,x} = 0 \tag{60}$$

$$\left(\frac{1}{80}c^4w_{2,tt} + \frac{1}{12}c^2w_{0,tt}\right)M_c - M_{Q2xc,x} + 2M_{zc} - M_{Q2yc,y} + \frac{1}{4}\lambda_{zt}c^2 - \frac{1}{4}\lambda_{zb}c^2 = 0 \tag{61}$$

The compatibility equations read:

$$-u_{0t} + \frac{1}{2}d_tw_{t,x} + u_0 - \frac{1}{2}u_1c + \frac{1}{4}c^2u_2 - \frac{1}{8}u_3c^3 = 0 \tag{62}$$

$$u_{0b} + \frac{1}{2}d_bw_{b,x} - u_0 - \frac{1}{2}u_1c - \frac{1}{4}c^2u_2 - \frac{1}{8}u_3c^3 = 0 \tag{63}$$

$$-v_{0t} + \frac{1}{2}d_tw_{t,y} + v_0 - \frac{1}{2}v_1c + \frac{1}{4}c^2v_2 - \frac{1}{8}v_3c^3 = 0 \tag{64}$$

$$v_{0b} + \frac{1}{2}d_bw_{b,y} - v_0 - \frac{1}{2}v_1c - \frac{1}{4}c^2v_2 - \frac{1}{8}v_3c^3 = 0 \tag{65}$$

$$-w_t + w_0 - \frac{1}{2}w_1 c + \frac{1}{4}c^2 w_2 = 0 \tag{66}$$

$$w_b - w_0 - \frac{1}{2}w_1 c - \frac{1}{4}c^2 w_2 = 0 \tag{67}$$

where the high-order stress resultants in the core equal:

$$\begin{aligned} &\{Q_{xc}, M_{Q1xc}, M_{Q2xc}\} = \int_{-\frac{c}{2}}^{\frac{c}{2}} (1, z_c, z_c^2)\tau_x \, \mathrm{d}z_c, \quad \{Q_{yc}, M_{Q1yc}, M_{Q2yc}\} = \int_{-\frac{c}{2}}^{\frac{c}{2}} (1, z_c, z_c^2)\tau_y \, \mathrm{d}z_c, \\ &\{M_{zc}, R_{zc}\} = \int_{-\frac{c}{2}}^{\frac{c}{2}} (1, z_c)\sigma_{zz} \, \mathrm{d}z_c \end{aligned} \tag{68}$$

The number of equations along with the compatibility equations is twenty-three. Notice that some of the equations are algebraic which means that this set of equations is a DAEs (differential–algebraic equations) set and not an ordinary PDEs set. All equations of motion in the core, Eqs. (51)–(61), are described in the integral sense and not in the differential one, see Eq. (16). In other words, a core with a shear free edge is defined here by null high-order stress resultants rather than by the condition of null shear stresses.

The boundary conditions, at each edge of the panel, consist of eleven conditions and the corners boundary conditions. Eight conditions out of the eleven are those of the upper and the lower face sheets, see Eqs. (18)–(28), and three additional ones are those of the core. The boundary conditions for the face sheets differ only by the shear boundary conditions in each direction; see Eqs. (21) and (22) for the x-direction, and Eqs. (26) and (27) for the y-direction. Only the different and additional boundary conditions are presented and they read:

The shear boundary conditions for the upper and the lower face sheets, at $x = 0$ or a (instead of Eqs. (21) and (22)) equal:

$$\lambda_{bc}\left(w_{t,xtt} I_{mt} + \frac{1}{2}\lambda_{xt} d_t + 2M_{xyt,y} + M_{xxt,x}\right) = V_{xt,\mathrm{ext}} \quad \text{or} \quad w_t = w_{t,\mathrm{ext}} \tag{69}$$

$$\lambda_{bc}\left(2M_{xyb,y} + \frac{1}{2}\lambda_{xb} d_b + w_{b,xtt} I_{mb} + M_{xxb,x}\right) = V_{xb,\mathrm{ext}} \quad \text{or} \quad w_b = w_{b,\mathrm{ext}} \tag{70}$$

And the shear conditions in the other direction, at $y = 0$ or b (instead of Eqs. (26) and (27)), read:

$$\lambda_{bc}\left(2M_{xyt,x} + \frac{1}{2}\lambda_{yt} d_t + w_{t,ytt} I_{mt} + M_{yyt,y}\right) = V_{yt,\mathrm{ext}} \quad \text{or} \quad w_t = w_{t,\mathrm{ext}} \tag{71}$$

$$\lambda_{bc}\left(w_{b,ytt} I_{mb} + \frac{1}{2}\lambda_{yb} d_b + M_{yyb,y} + 2M_{xyb,x}\right) = V_{yb,\mathrm{ext}} \quad \text{or} \quad w_b = w_{b,\mathrm{ext}} \tag{72}$$

The additional boundary conditions for the core, at $x = 0$ and a and $y = 0$ and b with $(j = x, y)$, read:

$$Q_{jc} = 0 \quad \text{or} \quad w_0 = w_{0,\mathrm{ext}} \tag{73}$$

$$M_{Q1jc} = 0 \quad \text{or} \quad w_1 = w_{1,\mathrm{ext}} \tag{74}$$

$$M_{Q2jc} = 0 \quad \text{or} \quad w_2 = w_{2,\mathrm{ext}} \tag{75}$$

where $w_{k,\mathrm{ext}} (k = 0, 1, 2)$ defines the external vertical displacement, rotation and curvature imposed at mid-height of the core, at $z_c = 0$.

The constitutive relations for each face sheet are those in the previous computational model and for the core those in Eq. (31). The stresses and the stress resultants in the core must be defined in terms of the displacements in order to describe the governing equations of motion in term of the unknown displacements. They are defined using the constitutive relations, Eq. (31) along with Eq. (68). Hence, they read:

Stresses:

$$\begin{aligned}\tau_{xc} &= G_{xc}(u_1 + 2u_2 z_c + 3u_3 z_c^2 + w_{0,x} + w_{1,x} z_c + w_{2,x} z_c^2)\\ \tau_{yz} &= G_{yc}(v_1 + 2v_2 z_c + 3v_3 z_c^2 + w_{0,y} + w_{1,y} z_c + w_{2,y} z_c^2)\\ \sigma_{zzc} &= E_{zc}(w_1 + 2w_2 z_c)\end{aligned} \tag{76}$$

Stress resultants:

$$\begin{aligned}Q_{xc} &= \frac{1}{12} G_{xc}(3u_3 + w_{2,x})c^3 + G_{xc}(u_1 + w_{0,x})c\\ M_{Q1xc} &= \frac{1}{12} G_{xc}(2u_2 + w_{1,x})c^3\\ M_{Q2xc} &= \frac{1}{80} G_{xc}(3u_3 + w_{2,x})c^5 + \frac{1}{12} G_{xc}(u_1 + w_{0,x})c^3\end{aligned} \tag{77}$$

$$\begin{aligned}Q_{yc} &= \frac{1}{12} G_{yc}(3v_3 + w_{2,y})c^3 + G_{yc}(v_1 + w_{0,y})c\\ M_{Q1yc} &= \frac{1}{12} G_{yc}(2v_2 + w_{1,y})c^3\\ M_{Q2yc} &= \frac{1}{80} G_{yc}(3v_3 + w_{2,y})c^5 + \frac{1}{12} G_{yc}(v_1 + w_{0,y})c^3\end{aligned} \tag{78}$$

$$R_{zc} = E_{zc} w_1, \quad M_{zc} = \frac{1}{6} E_{zc} w_2 c^3 \tag{79}$$

The governing equations of motion are formulated in terms of the following twenty three unknowns: the in-plane displacements of the mid-plane of the face sheets, in the x direction and y direction, the vertical deflections of the upper and the lower face sheets, the six Lagrange multipliers and the eleven polynomial coefficients of the core(see Eq. (43)). The first six equations are determined through substitution of the constitutive relations: see Eq. (30), in the equations of motion of the face sheets, Eqs. (45)–(50). The next eleven equations are derived through substitution of the stress resultant relations; Eqs. (77)–(79), into Eqs. (51)–(61). The additional six compatibility conditions remain unchanged. For the sake of brevity the governing equations of this model are not presented.

2.4. Free vibration of a simply-supported panel—model II

The free vibration of a simply-supported sandwich panel is presented next for the second computational model. The sandwich panel construction, used here, consists of face sheets that are specially orthotropic construction with unsymmetrical laminated composite materials, similar to the construction used in the formulation of model I. A closed-form solution exists also for this case and it is based on trigonometric functions for a harmonic excitation, which fully satisfy the boundary conditions, including those of the higher-order of the core. The solution is demonstrated for a one term since the Fourier series coefficients are independent.

The solution series reads ($j = t, b$):

$$
\begin{aligned}
u_{0j}(x,y,t) &= \left(\sum_{n=1}^{N}\left(\sum_{m=1}^{M} C_{u_{0j}}^{mn}\cos(\alpha_m x)\sin(\beta_n y)\right)\right)\mathrm{e}^{(\omega t I)}\\
v_{0j}(x,y,t) &= \left(\sum_{n=1}^{N}\left(\sum_{m=1}^{M} C_{v_{0j}}^{mn}\sin(\alpha_m x)\cos(\beta_n y)\right)\right)\mathrm{e}^{(\omega t I)}\\
w_{j}(x,y,t) &= \left(\sum_{n=1}^{N}\left(\sum_{m=1}^{M} C_{w_{j}}^{mn}\sin(\alpha_m x)\sin(\beta_n y)\right)\right)\mathrm{e}^{(\omega t I)}\\
u_{k}(x,y,t) &= \left(\sum_{n=1}^{N}\left(\sum_{m=1}^{M} C_{u_{k}}^{mn}\cos(\alpha_m x)\sin(\beta_n y)\right)\right)\mathrm{e}^{(\omega t I)} \quad (k=0,1,2,3)\\
v_{k}(x,y,t) &= \left(\sum_{n=1}^{N}\left(\sum_{m=1}^{M} C_{v_{k}}^{mn}\sin(\alpha_m x)\cos(\beta_n y)\right)\right)\mathrm{e}^{(\omega t I)} \quad (k=0,1,2,3)\\
w_{l}(x,y,t) &= \left(\sum_{n=1}^{N}\left(\sum_{m=1}^{M} C_{w_{l}}^{mn}\sin(\alpha_m x)\sin(\beta_n y)\right)\right)\mathrm{e}^{(\omega t I)} \quad (l=0,1,2)\\
\lambda_{xj}(x,y,t) &= \left(\sum_{n=1}^{N}\left(\sum_{m=1}^{M} C_{\lambda_{xj}}^{mn}\cos(\alpha_m x)\sin(\beta_n y)\right)\right)\mathrm{e}^{(\omega t I)}\\
\lambda_{yj}(x,y,t) &= \left(\sum_{n=1}^{N}\left(\sum_{m=1}^{M} C_{\lambda_{yj}}^{mn}\sin(\alpha_m x)\cos(\beta_n y)\right)\right)\mathrm{e}^{(\omega t I)}\\
\lambda_{zj}(x,y,t) &= \left(\sum_{n=1}^{N}\left(\sum_{m=1}^{M} C_{\lambda_{zj}}^{mn}\sin(\alpha_m x)\cos(\beta_n y)\right)\right)\mathrm{e}^{(\omega t I)}
\end{aligned}
\tag{80}
$$

where $C_{f_j}^{mn}(f_j = u_{0t}, v_{0t}, w_t, u_{0b}, v_{0b}, w_b, u_{0,1,2,3}, v_{0,1,2,3}, w_{0,1,2}, \lambda_{xt}, \lambda_{yt}, \lambda_{zt}, \lambda_{xb}, \lambda_{yb}, \lambda_{tb})$ are the constants of the series solution to be determined.

The solution is determined through substitution of a general term of the series, Eq. (80), into the governing equations of motion, which yields a set of homogeneous algebraic equations for each term of the series, instead of the partial differential—algebraic set of equations. Thus, the solution of the DAEs is replaced by an eigenvalue problem, with a mass and a stiffness matrix. Here, the dimension of the stiffness matrix is twenty three, while that of the mass matrix is seventeen only. However, since the set of equations is partially algebraic and partially differential equations, the corresponding mass and the stiffness matrices can be condensed into a dimension of 11 by removing the following dependent variables: $C_{\lambda_{xt}}$, $C_{\lambda_{yt}}$, $C_{\lambda_{zt}}$, $C_{\lambda_{xb}}$, $C_{\lambda_{yb}}$, $C_{\lambda_{zb}}$, $C_{u_{2,3}}$, $C_{v_{2,3}}$, $C_{w_{1,2}}$. Thus, the number of eigenvalues, for specified values of m and n is only eleven. Six out of these eleven eigenfrequencies are similar to those of the first computational model and the additional five correspond to local modes in the core, with nearly null displacements in the face sheets.

3. Numerical study

The numerical study demonstrates only some of the capabilities of the proposed computational models and is not a full blown parametric study which is beyond the scope of the paper. The study includes the free vibration behavior of two typical sandwich panels and a parametric study. The first panel consists of a symmetrical construction of a compressible sandwich panels and is presented only to validate of the results

of the two computational models. It has been compared with the following computational models: the Classical Plate Theory (CPT), the First-Order Shear Deformable Plate Theory (FOSDPT), the High-Order Shear Deformable Plate Theory (HOSDPT) due to Reddy and the general Third-Order Shear Deformable Plate Theory (TOSDPT), see Reddy (1997). The second one consists of a non-symmetrical construction of a compressible sandwich panels and it discusses the effect of the weight and rigidity of the core on the eigenfrequencies and eigenmodes. The parametric study investigates the effect of the rigidity of the core and its mass on the fundamental frequency.

The non-dimensional eigenfrequencies of a square simply-supported panel, $a = b = 1200$ mm, that consists of two identical glass fibers face sheets with a quasi-isotropic lay-up and a "soft", are presented first. The face sheet properties consist of thickness of $d_t = d_b = 6$ mm, an equivalent elastic modulus of 18 000 MPa and a density of 2000 kg/m^3. The core is isotropic, 60 mm thick, a light Divinycell foam core, HD100, with closed cells. Its properties are: $E_{zc} = 85$ MPa, $G_{xc} = 16$ MPa and a density of 100 kg/m^3. The eigenfrequencies of the proposed computational models, (with $m = n = 1$) are non-dimensioned with respect to first eigenfrequency of the CPT that is denoted by $\omega_{\text{classical}}$, have been compared with the various plate models and appear in Table 1. The results of the proposed models compare very well the results of the various plate theories. The lowest fundamental eigenfrequency of model II is very close to that of the TOSDPT while those of model I(HSAPT) and that of Reddy's plate theory are almost identical. The difference in the fundamental eigenfrequency between the two models is about 10–15%. Please notice that the proposed computational models are also able to detect higher eigenfrequencies such as Mode 6 in the first model and the last six modes in the second models, which the various plate theories along with the high-order ones lack.

The second case consists of a sandwich plate with unidentical laminated composite face sheets and two types of "soft" cores. The dimensions and the geometrical and mechanical properties of the face sheets are the same as in previous case except that $d_t = 12$ mm and $d_b = 6$ mm. The core is isotropic, 60 mm thick, a Divinycell foam core of type HD with closed cells. In order to study the entire spectrum of foam core, from the lightest to the heaviest one, two types of core are investigated: the light one, HD100, used in previous case, and the heaviest one HD250 with $E_{zc} = 300$ MPa, $G_{xc} = 110$ MPa and a density of 250 kg/m^3. The six and the eleven non-dimensional eigenfrequencies,(for $m = n = 1$), for the two computational models, relative to the lower eigenfrequency of an equivalent panel without shear rigidity(CPT), $\omega_{\text{classical}}$, appear in Table 2. In addition, the first three eigenfrequencies of the CPT model and the first five values of the FOSDPT model are included in Table 2 for comparison. Please notice that the lowest eigenfrequency of the FOSDPT is a little bit higher then that of model II and is about 13% lower then that of model I. The results for Modes 2–5 in the FOSDPT and the two models are almost identical. The discrepancy between the

Table 1
Non-dimensional eigenfrequencies, $\omega/\omega_{\text{classical}}$, of the various plate theories and the two computational models for $m = n = 1$ for a sandwich panel with identical face sheets

Mode no.	CPT	FOSDPT	HOSDPT (Reddy)	TOSDPT	Model I	Mode II
1	1.0	0.46401875	0.50421562	0.45347050	0.50180037	0.45452487
2	4.86631712	4.86631712	4.86631712	4.80007470	4.86631712	4.82949225
3	8.22557725	7.005830095	7.249152414	6.969566926	7.27446123	7.265180327
4		8.225577251	8.225577251	7.846011948	8.22555405	8.025359024
5		10.02899867	10.12998446	10.02681448	10.1843184	10.15749199
6				14.11246731	11.6602411	11.65827929
7				14.76569461		18.37957674
8				20.64946999		18.69890927
9				21.14437323		35.12724995
10						35.16621182
11						42.06247918

Table 2
Non-dimensional eigenfrequencies, $\omega/\omega_{classical}$, of the two models for various Divinycell foam cores and $m = n = 1$ for a sandwich panel with non-identical face sheets (unsymmetrical construction)

Mode no.	HD100				HD250			
	CPT	FOSDPT	Model I	Model II	CPT	FOSDPT	Model I	Model II
1	1.0	0.3959595662	0.4529651387	0.3923174974	1.0	0.747158039	0.7881577689	0.6796957532
2	4.946191356	4.946191356	4.899705631	4.870032709	4.999933176	4.999933176	4.865312339	4.861394596
3	8.360589333	6.338863250	6.66532645	6.654904339	8.451429596	8.451429596	8.220251375	8.200686944
4		8.360589333	8.263466507	8.093193471		10.94711203	12.21370097	12.20259205
5		9.444754025	9.657391600	9.633711841		13.02291024	14.05761391	14.03409186
6			9.856700373	9.850703953			18.35908648	18.34931763
7			–	17.51824641			–	45.29943517
8			–	17.77870281			–	45.38067221
9			–	33.98547029			–	74.76959640
10			–	34.01228285			–	88.32415740
11			–	40.14799270			–	88.36621342

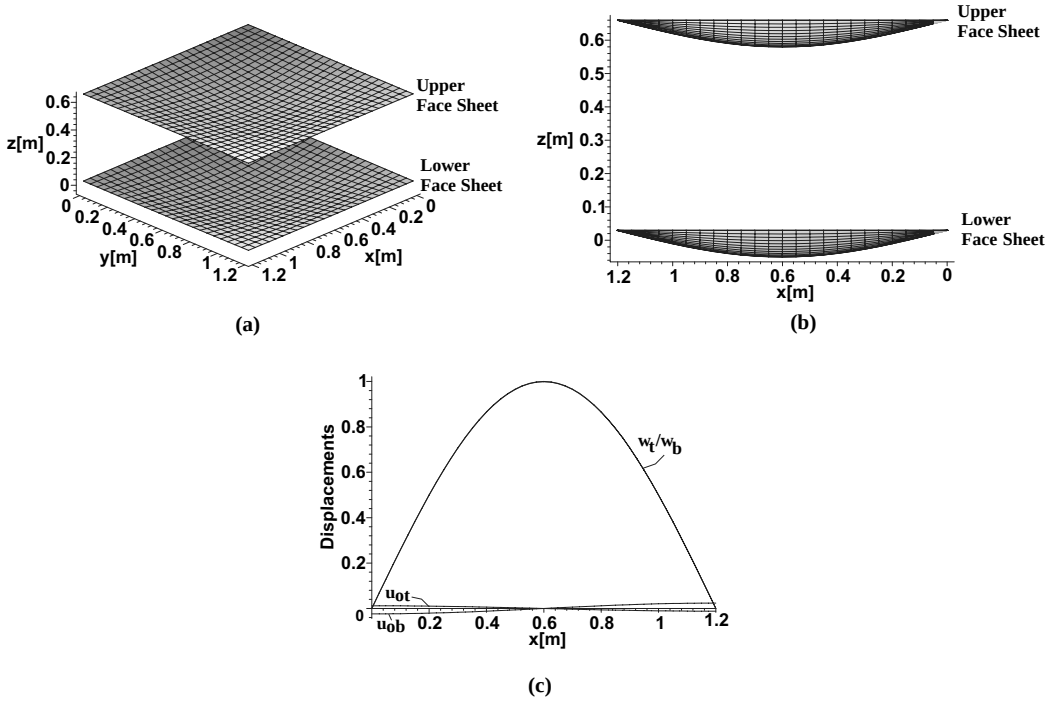

Fig. 3. Overall bending pattern—first eigenmodes (unsymmetrical construction): (a) 3D description, (b) view on the x–z plane, (c) in-plane and vertical displacements of face sheets through mid-span at $y = b/2$.

eigenfrequencies of the two computational models is only in the first mode and it is about 13%. The first six eigenmodes in the two models are identical. The last five eigenfrequencies (Modes 7–11) are higher modes, involving mainly displacements in the "soft" core, and can be determined only by the second computational model. Please note that they consist of pairs of eigenfrequencies that are very close.

The first, the third, and the sixth modes for $m = n = 1$ of the case with the HD100 core appear in Figs. 3–5. In Fig. 3 the overall bending mode, which corresponds to the first eigenmode, is described. The figure

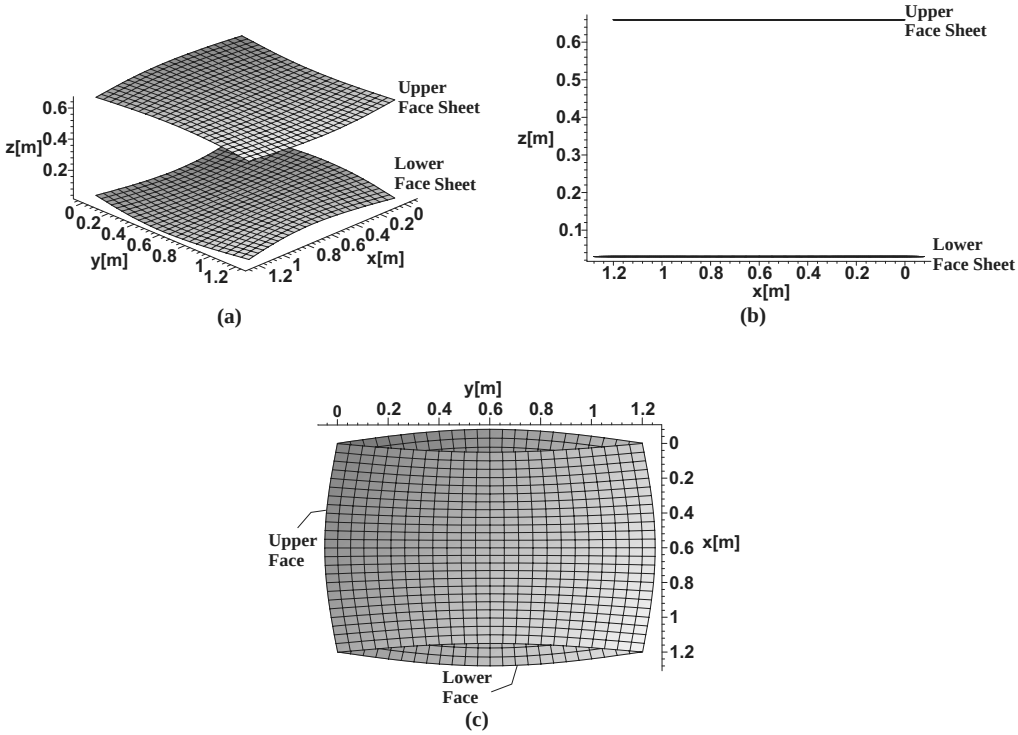

Fig. 4. Local in-plane pattern—third eigenmodes (unsymmetrical construction): (a) 3D description, (b) view on the x–z plane, (c) view on the x–y plane.

includes a 3D description of the mode, a view on the x–z plane and the displacements of the face sheets at mid-span at $y = b/2$. In Fig. 4 the eigenmodes of local in-plane displacements of the upper and the lower face sheets are presented. The 3D picture appears in Fig. 4a and views of the various planes appear in Fig. 4b and c. The in-plane displacements of the various face sheets, see Fig. 4c, reveal that the upper and the lower faces are distorted one perpendicular to the other. The pumping mode appears in Fig. 5 and it corresponds to the sixth eigenmode. The figure includes the 3D description and a view on the x–z plane. Fig. 5c describes the displacements curves at mid span, at $y = b/2$, and it reveals that the upper and the lower face sheets move opposite to each other in local bending.

The distributions of the displacements of the core, at its sides and mid-span and through its depth, of the first six eigenmodes, in longitudinal, transverse and vertical directions, appear in Fig. 6. The results reveal that the distribution of the vertical displacements are constants for the first five modes and linear for the sixth mode and those of the in-plane displacements are linear for the first mode, slightly non-linear for Modes 3 and 5 and non-linear for the even (Modes 2, 4 and 6). The linear distributions are in agreement with the first computational model assumptions that the distributions of the accelerations of the core through its depth are linear, see Eq. (9). Please note that although the in-plane acceleration distributions of the first computational model are linear the discrepancy between the eigenfrequencies of the two computational models is very small with the higher modes that consist of non-linear in-plane displacements distributions. This means that the rotary inertia of the core, which affects the behavior through the linear and non-linear in-plane displacements distributions, has a very minor effect on the eigenfrequencies. Or in

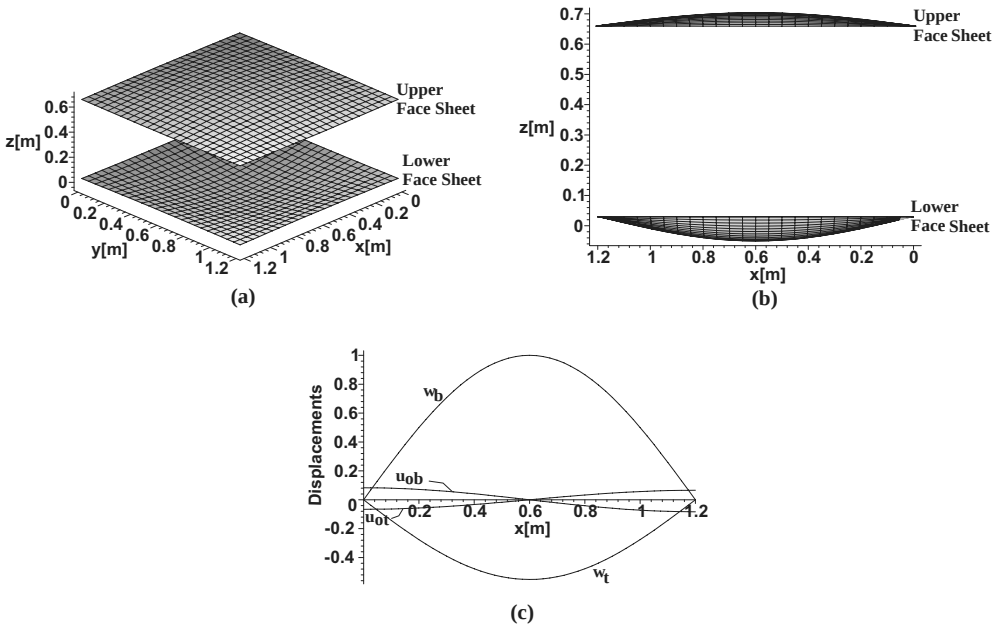

Fig. 5. Local bending pattern—sixth eigenmodes (unsymmetrical construction): (a) 3D description, (b) view on the x–z plane, (c) in-plane and vertical displacements of face sheets through mid-span at $y = b/2$.

other words, the main contribution of the core, to the free vibration of the panel, is due to its linear vertical displacements distribution.

The higher modes, Modes 7 and 11, which mainly involve displacements in the core, appear in Figs. 7 and 8. Each figure includes a 3D description of the deformed core and sections views in x and y directions that include: the displacements of the mid-height plane of the core as well. The in-plane displacements of the upper and the lower face sheets are very small and are not presented. The seventh mode involves in-plane displacements of the edges planes of the core, see Fig. 7b and c, with no vertical displacements. On the other hand, the eleventh mode involves pumping type of displacements also within the core, see Fig. 8, and with very small in-plane displacements, see Fig. 8b and c. This higher mode differs from the sixth mode, see Fig. 6, in terms of linear distributions of the vertical displacements and the no-linear displacements of the in-plane ones.

The distributions of the displacements of the core, at the side and mid-span of the panels and through its depth, of the last five eigenmodes (Modes 7–11), in the longitudinal, transverse, and vertical directions through its depth, appear in Fig. 9. The results reveal that the distribution of almost all displacements is non-linear except for the first four (Modes 7–10) in the vertical direction that are linear. The vertical displacements reach very large values at the eleventh mode only, while those of the in-plane ones reach extreme values at the seventh and eighth modes only. Here, the results and the assumption of the non-linearity of the distributions of the accelerations of the second computational model, see Eq. (43), coincide.

The parametric study investigates the effects of the ratio of the core modulus of elasticity relative to that of the face sheets on the lower eigenfrequency and it also validates the lower eigenfrequency result of the computational models. The study has been conducted on a square simply-supported panel of $a = b = 1200$ mm, with graphite epoxy quasi-isotropic face sheets of $d_t = d_b = 1.0$ mm in thickness, and an equivalent

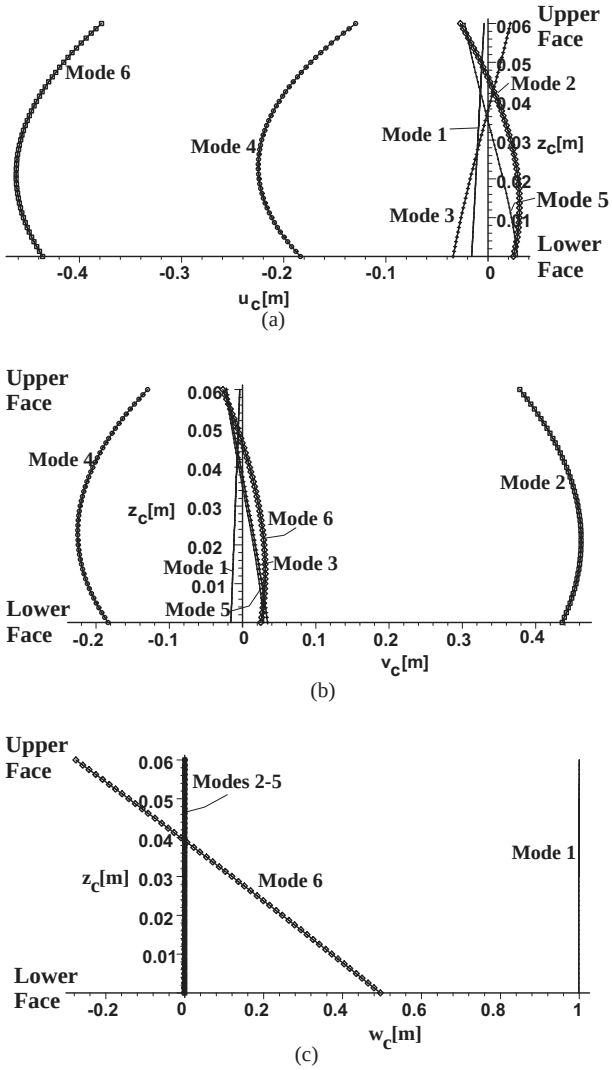

Fig. 6. Distributions of core displacements through its thickness (Modes 1–6, unsymmetrical construction): (a) displacement in x-direction (at $y = 0, x = a/2$), (b) displacements in y-direction (at $x = 0, y = a/2$), (c) vertical displacements (at $x = a/2, y = b/2$).

modulus of elasticity of $E_t = E_b = E_s = 27420$ MPa. The core is isotropic with a height of $c = 57.15$ mm and its density is related to the elastic modulus of elasticity of the core $\rho_c = 1.0805E_c(E_c$ in MPa). The ratio of E_c/E_s has been changed between the values of 1/1000 to 1/10, from the very light core(foam type) to the very heavy one(honeycomb type). The results of the lower eigenfrequency with respect to the lower eigenfrequency of an equivalent plate with flexural rigidity only appear in Fig. 10 in four curves. The first and the second curves describe the eigenfrequency of the first-order theory for isotropic plates, denoted by first-order (isotropic) and orthotropic plates which neglects the in-plane and the flexural rigidity of the core, denoted by first-order (orthotropic). The first-order eigenfrequency is calculated with the aid of the equation that appears on page 373 (Eq. (7.137)) in the book by Shames and Dym (1991) using a shear factor of 1 and a shear modulus that equals that of the core. In Fig. 10a the results are presented for the

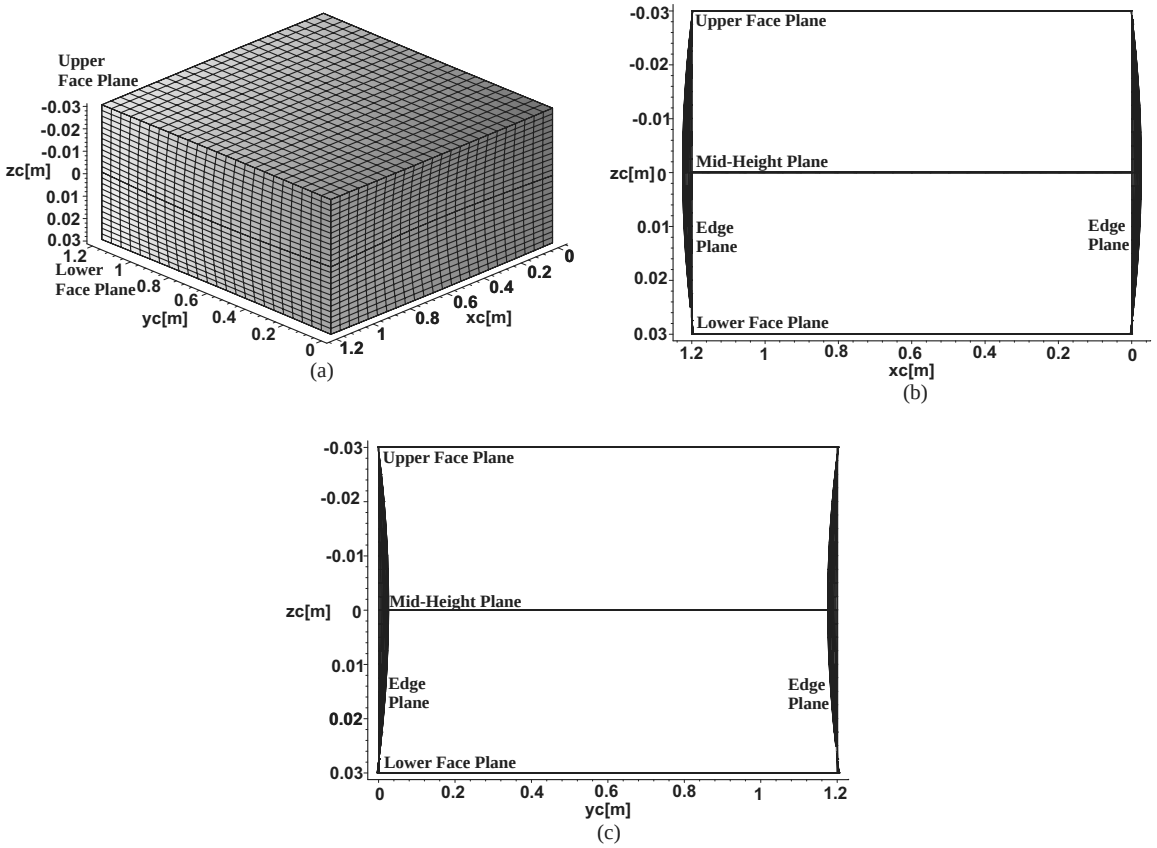

Fig. 7. Core modes—seventh mode (model II, unsymmetrical construction): (a) 3D description, (b) section view, x–z plane, (c) section view, y–z plane.

entire region of possible values of moduli ratios E_c/E_s, valid for cores made of foam or metallic honeycomb. Please note that the results of the first-order model(orthotropic) and those of model I coincide throughout the entire range which also validates the accuracy of the lowest eigenfrequency of the computational models. In Fig. 10b the region of moduli ratio is zoomed to the foam type of cores. The results of model I and the results for the first-order(orthotropic) coincide. In the foam core region, see Fig. 10a, the difference between all computational models is minor. The lowest values are those of the second computational model. As the core ratio increases the results of the two computational models have identical trends. The results of the first-order(isotropic) model are valid for very small values of E_c/E_s and as they increase, corresponding to heavy metallic honeycomb core, the discrepancy enlarges, up to 30%. This discrepancy is a result of the in-plane and flexural rigidity of the core that the first-order(isotropic) model takes also into account which the other computational models neglect. The results of the first-order(orthotropic) model that appear in Fig. 10a and Fig. 10b coincide with the results of the computational model I. Neglect of these rigidities is accurate whenever honeycomb types of panels are considered, since the in-plane rigidities of the honeycomb cells are null. The maximum lower eigenfrequency for this panel is reached when the moduli ratio is about 1/50 and descends for smaller and larger ratio values.

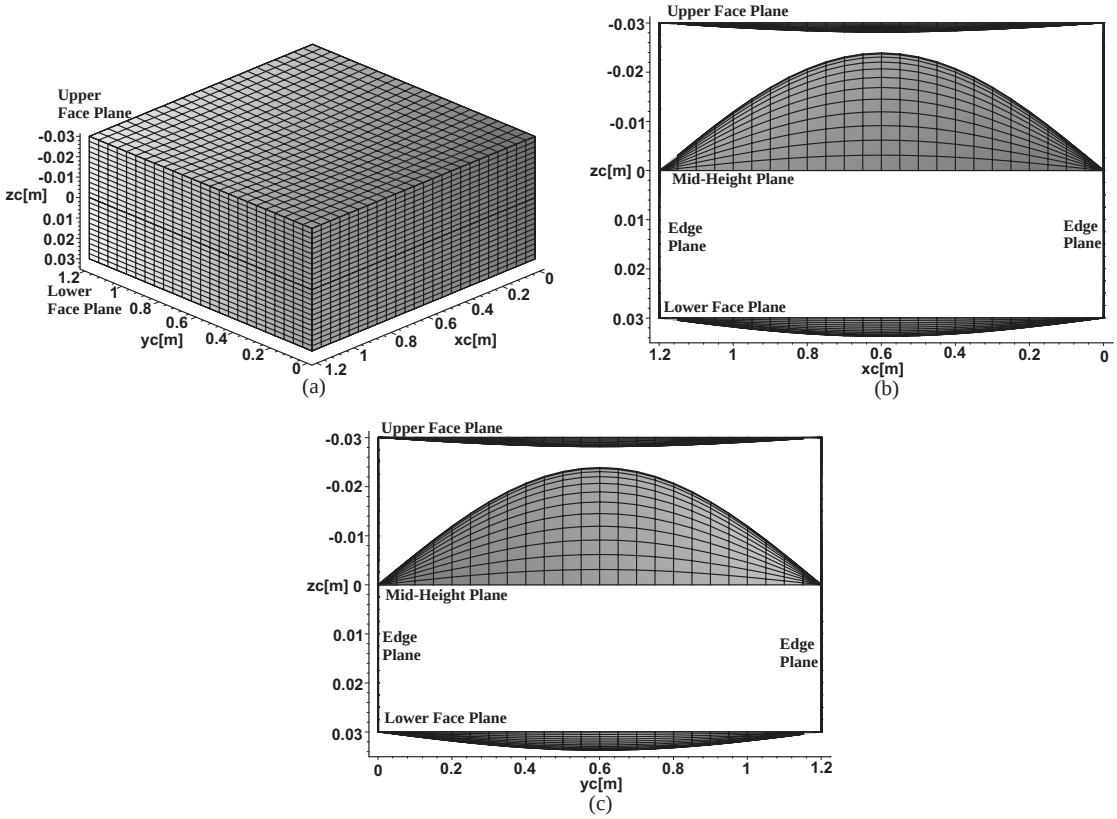

Fig. 8. Core modes—eleventh mode (model II, unsymmetrical construction): (a) 3D description, (b) section view, x–z plane, (c) section view, y–z plane.

4. Conclusion

A rigorous systematic free vibration analysis of sandwich panels with a flexible core that uses the high-order theory in computational models is presented. The mathematical formulation uses the Hamilton principle to derive the equations of motion along with the appropriate boundary conditions that include also rotary inertia terms. The formulation is general and is valid for any type of core, for any type of boundary conditions as well as the cases where the conditions at the upper face sheet are different from the lower one at the same edge, and to any type of loading, distributed or localized. The model yields results in the form of displacements, stress resultants in the face sheets, displacements and stress fields in the core, as well as interfacial vertical normal stresses at the core–face interfaces. Two computational models are presented.

The first computational model uses the shear stresses in the core as unknowns in addition to the face displacement ones. It assumes that the core transfers its inertia loads to the adjacent face sheets, and that the velocities and the accelerations distributions through its depth are assumed to be linear only to determine the kinetic energy contribution. The resulting displacement distributions in the core are non-linear, in general, and they take a cubic polynomial distribution for the in-plane displacements and a quadratic shape for the vertical displacements. The equations of motion consist of eight equations with the

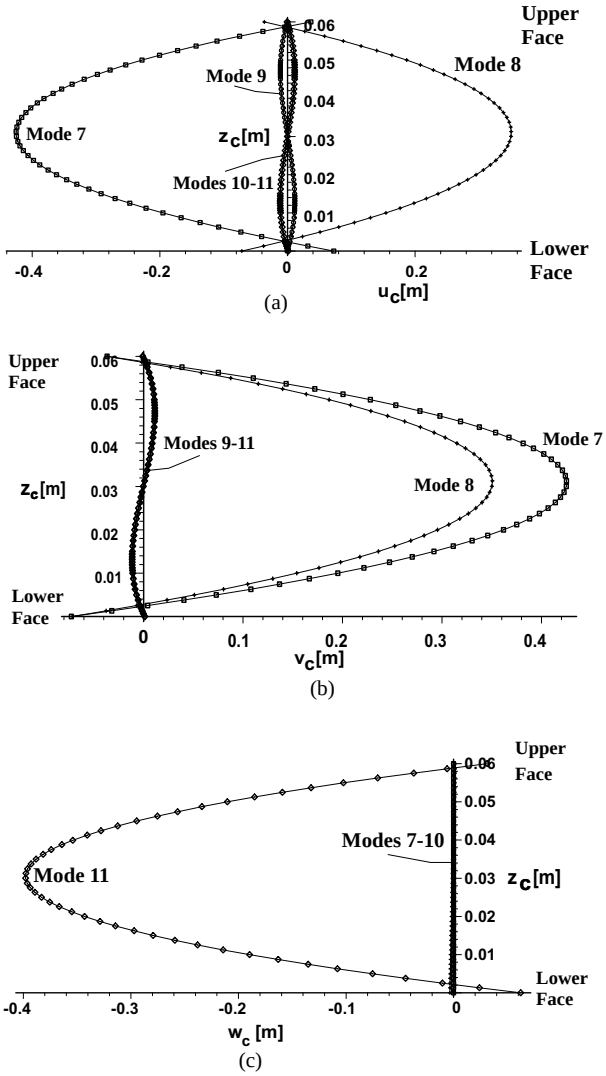

Fig. 9. Distribution of Core displacements through its thickness (Modes 7–11, model II, unsymmetrical construction): (a) displacement in x-direction (at $y = 0, x = a/2$), (b) displacements in y-direction (at $x = 0, y = a/2$), (c) vertical displacements (at $x = a/2, y = b/2$).

order of twenty. Closed-form solutions are presented for a simply-supported panel with specially orthotropic and an unsymmetrical lay-up of laminated composite material face sheets, along with the mass and stiffness matrices. The stiffness matrix dimension is eight while that of the mass matrix is only six. For each pair of wave numbers, m and n, there are only six eigenfrequencies.

The second computational model determines the effects of the discrepancy between the velocities of the core and the resulting displacements on the eigenfrequencies and the eigenmodes. It uses the displacements of the upper and the lower face sheets as unknowns, with the coefficients of the cubic and the quadratic displacement distributions of the core, which have been determined in the first model, and the Lagrange multipliers that are used to impose compatibility between the face sheets and the core at their interfaces. This formulation yields twenty-three equations of motions, algebraic and partial differential equations,

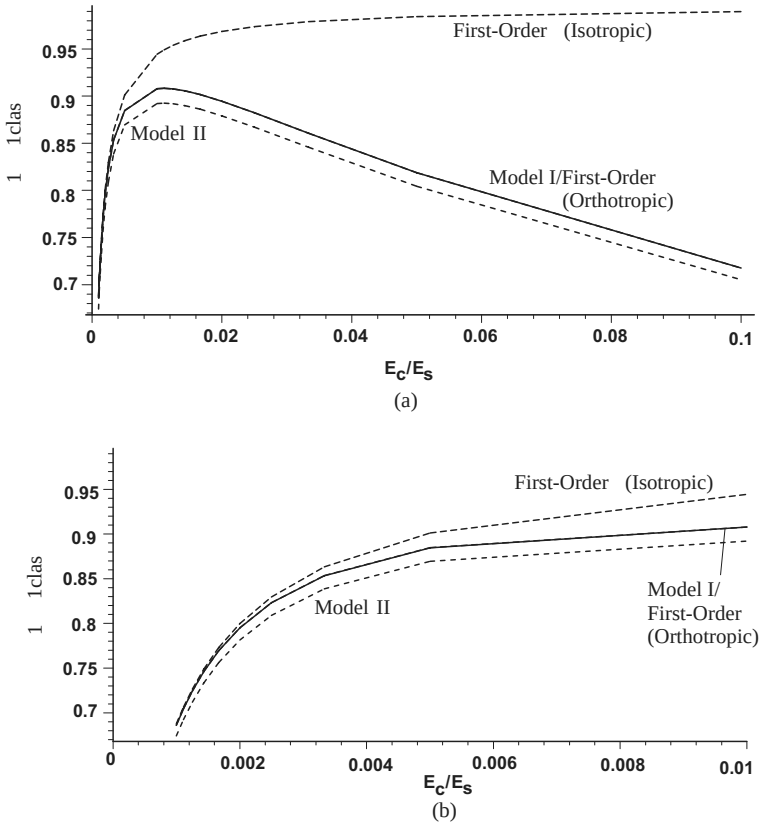

Fig. 10. Lower non-dimension eigenfrequency versus elastic moduli ratio of core to face sheets: (a) foam and honeycomb type of core region, (b) foam type of core region.

along with twenty-two boundary conditions in each direction. The closed-form solutions of a simply-supported panel with specially orthotropic and unsymmetrical face sheets yield a stiffness matrix with a dimension of twenty-three and a mass matrix with a dimension of seventeen. The number of valid eigenvalues even reduces to eleven since some of the unknowns are algebraic ones. The disadvantage of this model is that there are higher order stress resultants in the core that have only a mathematical meaning and are physically meaningless. In addition, it is nearly impossible to impose a real shear-free edge of the core with this model.

Some typical sandwich panels have been numerically investigated using the two computational models along with first-order and high-order plate theories for comparison and several eigenmodes are presented. The results of the various plate theories compared very well with those of the two computational models compared in the fundamental model as well as in the higher modes. A comparison between the results of the two computational models reveals a difference at the lowest eigenfrequency by about thirteen percent and very small differences for all other modes. All other higher eigenfrequencies are almost identical and in the two models the first six eigenmodes are almost identical, although the accelerations in the first model are linear, and in the second one, non-linear. Please notice that the eigenfrequencies of the second model are smaller then the corresponding ones in the first model. The second model yields additional modes which correspond mainly to displacements in the core along with very small displacements in the face sheets. The

lower values of the eigenfrequencies in the second model are a result of the additional degrees of freedom, in the formulation, as compared with the first computational model.

A parametric study has been conducted for a specific sandwich panel with graphite epoxy laminated composite face sheets. This study validates the accuracy of the lower eigenfrequency of the computational models, and examines the influence of the moduli ratio between the core and the face sheets on this eigenfrequency. The range of the moduli ratio starts from very low strength foam type of core to the very high strength metallic honeycomb. The eigenfrequency increases from almost insignificant values up to a maximum at a moduli ratio of about 1/50, and it descends as the ratio increases. The parametric study reveals that the results of the first-order(isotropic) model are valid as long as low strength and low weight foam type of core is of concern. A comparison between the results of the low frequency of the proposed models and the results of the first-order(orthotropic), model is in very good agreement.

The two computational models yield nearly identical results in spite of the inconsistency in the description of the velocities/accelerations and the displacement distributions through the depth of the core in the first model. They compare very well with the various plate theories and they enhance the physical insight of free vibration of sandwich panels with a "soft" core and should be used whenever a sandwich construction consists of a low-strength core.

References

Allen, H.G., 1966. Analysis and Design of Structural Sandwich Panels. Pergamon Press, London.

Bardell, N.S., Dundson, J.M., Langley, R.S., 1997. Free vibration analysis of coplanar sandwich panels. Composite Structures 38 (1–4), 463–475.

Bozhevolnaya, E., Frostig, Y., 2001. Free vibration of curved sandwich beams with a transversely flexible core. Journal of Sandwich Structures and Materials 3 (4), 311–342.

Frostig, Y., Baruch, M., Vilnay, O., Sheinman, I., 1992. A high order theory for the bending of sandwich beams with a flexible core. Journal of ASCE, EM Division 118 (5), 1026–1043.

Frostig, Y., Baruch, M., 1993. Buckling of simply-supported sandwich beams with transversely flexible core a high order theory. Journal of ASCE, EM Division 119 (3), 476–495.

Frostig, Y., Baruch, M., 1994. Free vibration of sandwich beams with a transversely flexible core: a high order approach. Journal of Sound and Vibration 176 (2), 195–208.

Frostig, Y., Baruch, M., 1996. Localized load effects in high-order bending of sandwich panels with transversely flexible core. Journal of ASCE, EM Division 122 (11), 1069–1076.

Frostig, Y., 1998. Buckling of sandwich panels with a transversely flexible core—high-order theory. International Journal of Solids and Structures 35 (3–4), 183–204.

Frostig, Y., Simitses, G.J., 2002. Structural similitude and scaling laws for sandwich beams. AIAA Journal 40 (4), 765–773.

Kant, T., Mallikarjuna, 1989. A high-order theory for free vibration of unsymmetrically laminated composite and sandwich plates—finite element evaluation. Computers and Structures 32 (5), 1125–1132.

Kant, T., Swaminathan, K., 2001. Analytical solution for free vibrations for laminated composite and sandwich plates based on a higher-order refined theory. Composite Structures 53, 73–85.

Lee, L.J., Fan, Y.J., 1996. Bending and vibration analysis of composite sandwich plates. Computer and Structures 60 (1), 103–112.

Meunier, M., Shenoi, R.A., 2001. Dynamic analysis of composite sandwich plates with damping modelled using high-order shear deformation theory. Composite Structures 54, 243–254.

Mindlin, R.D., 1951. Influence of transverse shear displacement on the bending of classical plates. Transaction of ASME, Journal of Applied Mechanics 8, 18–31.

Nayak, A.K., Moy, S.S.J., Shenoi, R.A., 2002. Free vibration analysis of composite sandwich plates based on reddy's higher-order theory. Composites Part B: Engineering 33, 505–519.

Noor, A.K., Burton, W.S., Bert, C.W., 1996. Computational models for sandwich panels and shells. Applied Mechanics Review 49, 155–199.

Plantema, F.J., 1966. Sandwich Construction. John Wiley and Sons, New York.

Rabinovitch, O., Vinson, J.R., Frostig, Y., 2003. High-order analysis of sandwich panels with piezoelectric composite face-sheets and a soft core. AIAA Journal 41 (1), 110–118.

Reddy, J.N., 1984. Energy and Variational Methods in Applied Mechanics. John Wiley and Sons, Inc., New York.

Reddy, J.N., 1990. A review of refined theories of laminated composite plate. Shock and Vibration Digest 22 (7), 3–17.
Reddy, J.N., 1997. Mechanics of Laminated Composite Plates: Theory and Analysis. CRC Press, Boca Raton, FL.
Senthilnathan, N.R., Lim, S.P., Lee, K.H., Chow, S.T., 1988. Vibration of laminated orthotropic plates using a simplified higher-order displacement theory. Composite Structures 10, 211–229.
Shames, I.H., Dym, C.L., 1991. Energy and Finite Element Methods in Structural Mechanics, SI Units Edition, Taylor and Francis.
Sokolinsky, V., Frostig, Y., 2000. Branching behavior in the non-linear response of sandwich panels with a transversely flexible core. International Journal of Solids and Structures 37, 5745–5772.
Thomsen, O.T., Frostig, Y., 1997. Localized bending effects in sandwich panels: photoelastic investigation versus high-order sandwich theory results. Composite Structures 37 (1), 97–108.
Vinson, J.R., 1999. The Behavior of Sandwich Structures of Isotropic and Composite Materials. Technomic Publishing Co. Inc, Lancaster.
Wang, C.M., 1996. Vibration frequencies of simply-supported polygonal sandwich plates via Kirchhoff solutions. Journal of Sound and Vibration 190 (2), 255–260.
Whitney, J.M., 1987. Structural Analysis of Laminated Anisotropic Plates. Technomic Publishing Co., Lancaster.
Zenkert, D., 1995. An Introduction to Sandwich Construction. Chameleon Press Ltd., London.